Sandpiles, avalanches, and the statistical mechanics of nonequilibrium stationary states

Ashvin B. Chhabra
Computational and Applied Math Program, Department of Mathematics and The James Franck Institute, The University of Chicago, Chicago, Illinois 60637

Mitchell J. Feigenbaum
The Rockefeller University, York Avenue, New York, New York 10021

Leo P. Kadanoff
Computational and Applied Math Program, Department of Mathematics and the James Franck Institute, The University of Chicago, Chicago, Illinois 60637

Amy J. Kolan
Computational and Applied Math Program, Department of Mathematics and the James Franck Institute, The University of Chicago, Chicago, Illinois 60637 and St. Olaf College, Northfield, Minnesota 55057

Itamar Procaccia
Computational and Applied Math Program, Department of Mathematics and the James Franck Institute, The University of Chicago, Chicago, Illinois 60637 and Department of Chemical Physics, The Weizmann Institute of Science, Rehovot 76100, Israel

(Received 22 June 1992)

The scaling properties of three nontrivial one-dimensional avalanche models are analyzed. The first two of them are the local limited model with one open, one closed, and with periodic boundary conditions, respectively. A theory for the scaling properties of these models based on the existence of two fundamental length scales, which diverge in the thermodynamic limit, is developed. The third model studied is a trapless version of the nonperiodic local limited model. We find that it is scale invariant. Our theoretical predictions are compared with extensive computer simulations in all three cases.

PACS number(s): 05.40.+j, 02.50.−r, 64.60.−i

I. INTRODUCTION

A class of recently studied sandpile models [1], although not representative of real sand [2], are useful systems for studying the statistical mechanics of nonequilibrium transport processes. They are specified by adding on "grains" of sand in a random fashion and deciding what happens after each addition by using very simple rules of evolution. Their transport properties are reminiscent of nonequilibrium fluids, but they have an obvious advantage of not being governed by the Liouville equation, which is nonsoluble even for the simplest cases.

Cellular-automaton sandpile models were introduced in the work of Bak, Tang, and Weisenfeld [3,4], who suggested that the pile would adjust its slope to a critical value in which there would be a wide range of avalanche sizes. They suggested that such qualitatively similar behavior would occur in a wide variety of systems and called it "self-organized criticality." The aim of this paper is to analyze in some detail a number of related nontrivial sandpile models that exhibit rather unusual statistical mechanics, and to explore further the similarity of their statistical properties to those of nonequilibrium fluids.

The behavior of such models is very different depending on whether the rules of evolution are based on the absolute heights of the piles or whether they depend on the local slopes. In absolute height models, grains of sand are added one at a time at random locations on the lattice. When the height at a site exceeds a threshold value, a certain number of grains fall onto the site's nearest neighbors. This in turn makes some of the neighbors unstable, which then shed grains to their neighbors, thus setting off an avalanche. This process is repeated until the entire sandpile is stable and then the addition process starts again. Quantities of interest are the nature of the recurrent configurations and their number as a function of the system size, the distribution of avalanches, etc. In a series of elegant papers, Dhar [5,6] showed that a large class of absolute height models were Abelian, i.e., the addition processes commuted. This property leads to a particularly simple equiprobable partitioning in configuration space and allowed an exact solution of these models.

The models studied here do not have the Abelian property. The rules of evolution depend on the local slope rather than the local height. The main model that we explore was introduced and first studied in Ref. [1] (hereafter referred to as local limited or LL models). In this model, as soon as the local *slope* gets large enough, a local slide (from left to right) is started. This slide can add extra material downhill and thus trigger further events

below it. The displacement of material can also undermine the sand above it, which then can also start in motion causing backavalanches. The extent of the backavalanches is restricted by sites that possess zero or negative local slope (trapping sites) and by the left-hand boundary (an infinite wall). The backavalanches (which physically reflect the property that the sand at the bottom of the pile supports the sand at the top) are a feature introduced by considering local slopes rather than absolute heights.

We begin this paper by discussing the LL model and find that it is difficult to solve exactly because of two nonrelated features. The first is the existence of an average flux maintained by the boundary conditions, which makes the model not translationally invariant. The second difficulty stems from the nontrivial distribution of trapping sites, which in turn makes the distribution of avalanches difficult to calculate.

To guide us in our understanding of the scaling properties of the LL model we introduce two related models, each having only one of the two difficulties mentioned above. The first is the PLL (periodic local limited) model which is governed by the same rules as the LL model, except that the boundary conditions are now periodic. This model still has a nontrivial distribution of traps but is translationally invariant. The second is the LLL model (local limited, limited to no traps), which has rules analogous to those of the LL model, but disallows the formation of traps. Both simplified models are amenable to analyses whose results guide us in our understanding of the LL model.

In Sec. II, after reminding the reader of the rules of the LL model, we analyze its set of recurrent configurations. These are the configurations that are revisited during the course of time, and they define the space on which statistical mechanics is done in this model. It will be shown that the calculation of the number of recurrent configurations as a function of the system size maps onto classical problems in mathematics, like the Euler problem of polygon division and the Catalan problem, so one can exactly calculate the number of recurrent configurations in a system of size L. The probability to see a configuration in the course of time is uniquely determined by a Markov matrix of transitions probabilities. It is shown that, in contradistinction to the so-called Abelian models [5,6], here the probabilities of the various configurations are widely different, adding to the complexity and the interest of this class of models. Having found that, we turn then to a symbolic description of the configurations in terms of height differences, or local slopes. The description at each site has two parts, a binary spin variable which has trivial statistical properties, and the number of traps which has nontrivial statistics.

In Sec. III we shall present the PLL model. By repeating the sandpile periodically, we regain translational invariance, and turn the model to an essentially soluble problem. The main asset of this simplified model is that it allows us to understand the role of traps in limiting the extent of the correlations in these models. We develop a scaling theory which is based on the existence of two fundamental length scales. The first is the mean distance between trapping sites which scales like $L^{1/3}$. The second is a coherence length ξ, which scales like $L^{2/3}$. The predictions of the theory are checked against extensive numerical simulations.

In Sec. IV we use the results of the PLL model to construct a scaling theory of the LL model. To connect the results of the PLL model to the LL model, we shall argue that the PLL model is a microcanonical version of the canonical LL model. The scaling theory is tested against numerical simulations in Sec. V. It appears that our understanding of this model is in good (but not perfect) agreement with the simulations.

In Sec. VI we will present the LLL model. We solve the model in the mean-field Reynolds approximation, which we think captures much of the essence of the exact solution. It will become clear, in the course of the solution of this model, that the problem is truly very similar to the nonequilibrium behavior of fluids. We shall find that the calculation is identical in form to the hierarchical calculation in terms of correlation functions in fluid mechanics. A diffusion equation appears naturally in terms of slope variables, and its solution calls for approximating higher-order correlation functions in terms of products of lower-order ones, exactly like the closure approximation in fluid statistical mechanics. Due to the lack of traps, the correlation in the LLL model extend throughout the system. The power-law decay of the correlations, which is predicted by the theory, is tested and confirmed by numerical solutions.

Section VII offers a summary and a discussion. In this discussion we address the fundamental question of why long correlations build up in these systems. We will propose that the mechanism for creating the long correlations in these models is similar to the one operating in other nonequilibrium stationary states which support a nonzero average flux such as heat conducting fluids.

II. THE LOCAL LIMITED MODEL

A. Definition of the model

Consider a one-dimensional lattice of L sites, on which grains of "sand" are distributed one at a time with equal landing probability. Let the number of grains accumulated on the jth site be denoted by H_j. The rules of the LL model are that grains are free to accumulate as long as

$$H_j - H_{j-1} \leq 2 \quad \forall\ j = 1,2,\ldots,L\ . \tag{1}$$

When Eq. (1) is not obeyed, two grains fall from site j to site $j-1$. Note that the falling process is inherently asymmetric: grains fall only toward lower j. The process will continue until Eq. (1) is obeyed at all sites $j = 1,2,\ldots,L$. All unstable sites are updated simultaneously. Then a new grain is added randomly and the process continues. At one end of the pile there is a wall and at the other end there is an abyss. The boundary conditions on the sites 0 (abyss) and $L+1$ (wall) are therefore

$$H_0 = 0, \quad H_{L+1} = H_L\ . \tag{2}$$

These rules define the model completely.

B. Slides, avalanches, and the local slopes

In terms of observed behavior, an interesting quantity to measure is the number of grains that cascade down the slope or fall off the pile after every addition of a single grain. By working in new variables based on local slopes rather than absolute heights, we can predict these quantities immediately from knowledge of the configuration and where the sand was added.

Define the variables S_j (local slopes) and ϵ_j by

$$S_j = H_j - H_{j-1} , \tag{3}$$

$$\epsilon_j = S_j - 1 . \tag{4}$$

The variable ϵ_j can take on the values $1, 0, -1, -2, \ldots, -2j+1$. Sites with negative values of ϵ_j are termed hereafter as trapping sites (for reasons that will become clear in the next paragraph).

The rules of sandpile evolution are then as follows.

(R1) If the added grain hits a site with $\epsilon_j \leq 0$, it simply sits there, and ϵ_j increases by 1, whereas ϵ_{j+1} decreases by 1.

(R2) If the grain hits a site with $\epsilon_j = 1$, two grains fall to the right. The value of ϵ_i decreases by 1, whereas ϵ_{j+1} increases by 2. The pair of grains will continue to slide until they reach the first site on the right (say k) for which $\epsilon_j < 0$, at which point they come to a stop. This is why sites with negative values of ϵ_j are called trapping sites. If k does not correspond to the abyss, then ϵ_k increases by 2 and ϵ_{k+1} decreases by 2. If no such site is encountered, then the grains will fall into the abyss.

(R3) If a grain is added on a site with $\epsilon_j = 1$ and if $\epsilon_{j+1} = 1$, then there will be a displacement of sand that includes the entire layer (two grains thick) between the site that was hit and the first trapping site (say m) to the left of that site (as shown in Fig. 1). This layer will slide down until it hits the first trapping site (k) on the right. The net changes will be

$$\epsilon_j = \epsilon_j - 1, \quad \epsilon_{j+1} = \epsilon_{j+1} - 1, \quad \epsilon_m = \epsilon_m + 2 ,$$

$$\epsilon_k = \epsilon_k + 2, \quad \epsilon_{k+(j-m)} = \epsilon_{k+(j-m)} - 2 .$$

Should there be no trapping site on the right of the added grain, the entire layer will fall into the abyss, corresponding to an avalanche of size $m-j$. In particular, if $\epsilon_1 = \epsilon_2 = 1$, and if all other $\epsilon_j \geq 0$, then hitting with a grain on site 1 will produce an avalanche of size $2L$, which is the largest avalanche possible.

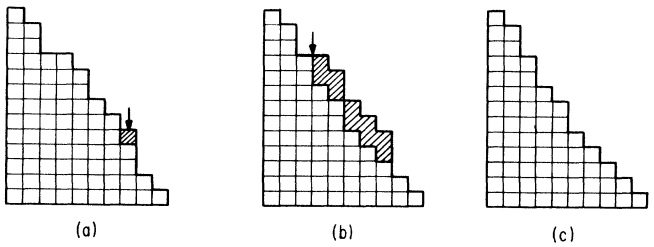

FIG. 1. Example of how an avalanche is created. (a) The arrow shows a grain being added on a site with a local slope of 2 whose left neighbor also has a local slope of 2. (b) The avalanche backpropagates until it reaches a site whose local slope is 0 or negative (denoted by an arrow). The shaded region shows the grains of sand that fall downhill as a result of this addition. (c) The sandpile after the avalanche. The entire shaded region in (b) has fallen off the edge corresponding to an avalanche of size 10 grains.

(R4) The boundary conditions are $\epsilon_{L+1} = -1$, $\epsilon_1 = H_1 - 1$.

These rules exhaust all the different possibilities. In particular, they imply that the model is integrable between successive additions of sand. Using them, we have been able to write rather efficient codes for simulating the transport behavior of this model. The above rules also reveal how traps are destroyed or created. In particular the addition of sand at a site will increase the slope of that site by one while reducing the slope of its left neighbor by the same amount. Similarly through an avalanche, the site at which the head of the avalanche comes to rest has its slope increased by 2, while the site where the avalanche started as well as the site which is the left neighbor to the tail of the avalanche have their slopes reduced by 2. These are the only ways traps are created or destroyed. It is not hard to convince oneself that the occurrence of deep traps (slope less than -1) is unlikely in this system.

C. Recurrent and nonrecurrent configurations

Not all of the stable configurations are recurrent in the dynamics. First, consider the number of different configurations that the sandpile can possess. For example consider a sandpile consisting of a single site $L=1$. Figure 2(a) is the Markov diagram corresponding to such a sandpile. The only current, stable values of H_1 are 1 and 2, whereas 0 is transient, and 3 is unstable. Figure 2(b) shows that for $L=2$ there are five recurrent configurations, which denoted as H_2H_1 take the values 21, 31, 22, 32, and 42. It is easy to see that the maximum height of a site at a distance x from the abyss, in a stable configuration of the sandpile is $2x$. This is because if the height difference between any two successive sites was greater than 2, that site would be unstable. Thus the local slope at each site can never be greater than 2, and the maximum average slope (averaged over the entire sandpile) is also 2. It is also not hard to convince oneself that the minimum slope for a recurrent configuration is one, and that a configuration is recurrent if each site is stable and

$$H_j \geq j . \tag{5}$$

A simple device for finding all the recurrent configurations for an arbitrary value of L is presented as a tree in Fig. 3. The branches are labeled by numbers, which for each group of branches starts with L and increases consecutively, reaching $2L$ only in the last group. The recurrent configurations for a system of size L are the values of $\{H_j\}$, which are obtained by reading the labels of the branches from top to bottom. The number of recurrent configurations is the number of branches on the Lth level of construction.

The number of recurrent states as a function of L forms a sequence of numbers (2,5,14,42,132,. . . for

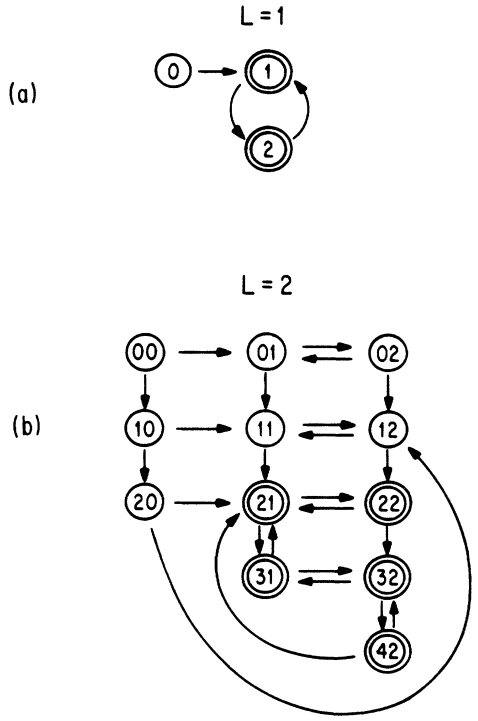

FIG. 2. Markov diagrams for (a) a single site and (b) a two site sandpile showing all the possible transitions of various configurations when a grain of sand is randomly added. The numbers in the middle of the circles are the heights at each site. Double circles denote recurrent configurations while single circles denote nonrecurrent ones.

$L=1,2,3,4,5,\ldots$) called the Catalan numbers (see Appendix A). This sequence was first generated by Euler in 1751 as the solution of the problem of how many ways can one divide a convex polygon into triangles by connecting vertices. These numbers are given by the formula

$$C(n)=\frac{1}{n+1}\binom{2n}{n}, \quad n\geq 0 . \tag{6}$$

For our case the number of recurrent states N_L is given by $N_L=C_{n=(L+1)}$. One can show that for large L, N_L goes as $4^L/L^{3/2}$. Now that we know the number of recurrent configurations we should discuss the probability of their occurrence.

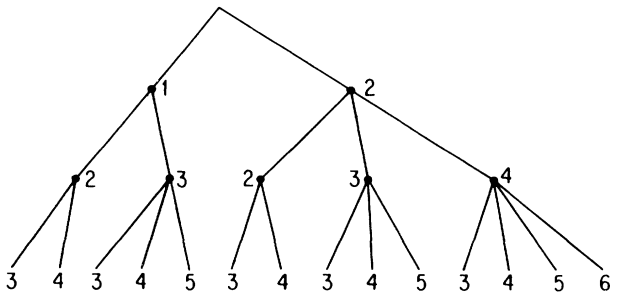

FIG. 3. Catalan tree: a compact hierarchical way to enumerate all the recurrent states of the sandpile. Each level of the tree represents an additional site being added. The numbers are the heights at each site. The construction of this tree is explained in the text.

D. The Markov matrix and the invariant probabilities

Upon the addition of one grain of sand a process of slides and avalanches can be triggered; however, the end result is simply a transition from one recurrent state $\{H_j\}$ to another recurrent configuration $\{H'_j\}$. Thus the dynamics can be fully described by a matrix of rank $N_L\times N_L$ with transition probabilities whose values are either zero or $1/L$. For example, for $L=1$ the Markov matrix is

$$\begin{pmatrix} 0 & 1 \\ 1 & 0 \end{pmatrix}, \tag{7}$$

where the rows and columns correspond to the recurrent configurations to heights 1 and 2. For $L=2$ the Markov matrix is

$$\begin{pmatrix} 0 & \frac{1}{2} & \frac{1}{2} & 0 & \frac{1}{2} \\ \frac{1}{2} & 0 & 0 & \frac{1}{2} & 0 \\ \frac{1}{2} & 0 & 0 & 0 & 0 \\ 0 & \frac{1}{2} & \frac{1}{2} & 0 & \frac{1}{2} \\ 0 & 0 & 0 & \frac{1}{2} & 0 \end{pmatrix}, \tag{8}$$

where the rows and columns correspond to the recurrent configurations 21,31,22,32,42. In these matrices, the columns always sum up to unity. Accordingly there exists a left eigenvector of eigenvalue 1, which is the unit vector. The right eigenvector of eigenvalue 1 is the stationary solution of the Markov chain, and its entries are the invariant probabilities for the recurrent configurations. Finding a solution for this eigenvector for an arbitrary L is equivalent to solving the LL model exactly.

The probabilities of *some* configurations can be found exactly, using the following thinking. Consider an arbitrary configuration. Assign an even (e) or odd (o) parity to each site depending on whether the height at each site is even or odd. The addition of a grain at any site will simply flip the parity of that site. Note that since avalanches always consist of pairs of grains, they do not change the parity of any site. Thus we can define a set of sum rules based on the parity at all sites in a configuration. For example, consider a two-site sandpile which, as we have discussed earlier, consists of five recurrent states. Of these three of them 21, 31, and 32 have unique parity states *eo*, *oo*, and *oe*, respectively. However, the configurations 22 and 42 have identical parity configurations (*ee*). Defining $P(H_2H_1)$ as the probability of the configuration H_2H_1 we get the following equations:

$$P(21)=P(31)=P(32)=\tfrac{1}{4} , \tag{9}$$

$$P(22)+P(42)=\tfrac{1}{4} . \tag{10}$$

Now the number of unique parity configurations increases as 2^L, while the number of recurrent states increases asymptotically as $4^L/L^{3/2}$. Thus this approach only provides partial information about the probabilities of various configurations and is increasingly less useful as L gets larger.

Since the number of configurations grows exponentially with system size, and since probabilities of the occurrence of these configurations is nontrivial, exact enumerations rapidly become impossible. We have not been able to find an exact solution to this problem. However, we will now proceed to develop a scaling theory, based on very general arguments, that captures the scaling behavior of these sandpiles in the thermodynamic limit.

E. Dynamics of the LL model

Let us think about the dynamics of the LL model as a two-step process. In the first part, the addition part, a grain of sand is added to a randomly chosen site. We visualize that this first step takes a time interval equal to $\frac{1}{2}$. In symbols, we have

$$H_j(t+\tfrac{1}{2})=H_j(t)+\eta(t) \quad \text{(addition step)} , \tag{11}$$

where $\eta_j(t)$ is a random variable which describes the addition process. It is defined so that

$$\eta_j(t)=\begin{cases}1 & \text{if sand is added on } j \\ 0 & \text{otherwise} .\end{cases} \tag{12}$$

The second step comes after the sand is added. We call this the avalanche step. Whenever the local slope S_j is greater than 2, sand will fall from site j to reappear on the downhill site $j-1$. This process will continue until there are no remaining slopes greater than 2, whereupon the process will terminate. The process can be summarized as

$$H_j(t+1)=H_j(t+\tfrac{1}{2})-2N_j+2N_{j+1} \quad \text{(avalanche step)} . \tag{13}$$

Here N_j is the number of times two grains fall downhill through the site j. Remember that the addition process always changes H_j or S_j by an odd number while the slide process changes these quantities by even numbers. We can learn a lot about the qualitative nature of the probabilities involved if we keep this concept clearly in mind. (Indeed, we used this observation to compute the probabilities of configurations with a unique parity configuration in Sec. II D). With this end in view define

$$S_j=1+\frac{(1+\sigma_j)}{2}-2M_j . \tag{14}$$

Here σ_j is a "spin variable" which takes on values ± 1 and M_j is a variable which describes the trap depth which takes on values 0 (when there is no trap), 1 (corresponding to slopes of 0 and -1), and occasionally higher integer values (corresponding to even deeper traps which for this model occur very rarely). The time development of the "spin" variable σ is quite simple indeed. The net effect of the addition is

$$\sigma_j(t+1)=\begin{cases}-\sigma_j(t) & \text{if grain is added on } j \text{ or } j-1 \\ \sigma_j(t) & \text{otherwise} .\end{cases} \tag{15}$$

The dynamics of the M_j's is more involved, but can be simply derived from the rules for updating ϵ that were discussed earlier.

Notice that most of the processes that go on respect a partial conservation law for the total slope

$$S_T=\sum_{j=1}^{L} S_j . \tag{16}$$

The average slope of the entire sandpile S_T is also the absolute height of the leftmost site of the sandpile divided by the length of the sandpile L. The height of the leftmost site changes only when either a grain of sand is added at $j=L$ or when a backavalanche reaches $j=L$. All other processes exactly conserve S_T. This conservation law can be restated as an equation of motion for M_j or S_j during the slide process. From Eqs. (1) and (13) during the slide process

$$\tfrac{1}{2}[S_j(t+1)-S_j(t+\tfrac{1}{2})]=-M_j(t+1)+M_j(t+\tfrac{1}{2}) =-2N_j+N_{j+1}+N_{j-1} . \tag{17}$$

From this point of view, the boundary condition at the bottom end is that

$$N_0=N_1 , \tag{18}$$

while that at the wall is

$$N_{L+1}=0 . \tag{19}$$

There is another crucial invariance. Notice that, although the addition process does change the σ_j's, the avalanche certainly does not. Moreover, the avalanche is totally unaffected by the values of these spin-parity variables. As a result, the σ_j's are uncorrelated and randomly distributed onto the values ± 1. This statement is rigorous. Less rigorously, one might say that it is reasonable to expect only a weak correlation between nearby values of M_j and σ_j.

III. THE PERIODIC LOCAL LIMITED MODEL

In the periodic model, each site is just the same as each other site, so that special conditions such as Eqs. (18) and (19) are omitted. Instead, we require periodicity for S, M, and σ, e.g., that

$$S_{j+L}=S_j . \tag{20}$$

The site at which the avalanche will come to a stop is found by moving away from the site at which sand was added (in a clockwise direction) and continuing until the first trap is encountered, using the periodicity if necessary. There is only one danger, which arises if a trap-free configuration is reached. Then an addition can cause grains to go around the sandpile endlessly. It is easy to devise a set of rules to deal with such a situation. Howev-

er, as a precaution to avoid biasing the natural dynamics of the sandpile in any way, in all our simulations we simply choose L large enough (i.e., start with enough traps) so that this situation is not reached within our simulation time.

The periodic model defined in this way has properties which are essentially similar to those of the LL model, so long as no processes extend over the entire length of the system. Nothing like this will happen as long as there are many traps in the system. In the LL model, all of the S_j's are uncorrelated and randomly distributed. The periodic boundary conditions cause only $L-1$ of the spins to be independently distributed. This correction, however, can be neglected in the thermodynamic limit, and so in our arguments we assume that all of the S_j's are uncorrelated and randomly distributed. Moreover, the conservation law on S_T is now exactly satisfied. The cost of the translational invariance in the PLL model is that, in addition to specifying L, now one must also specify the slope of the system. From Eq. (14), we see that

$$S_T=\frac{3}{2}L+\frac{\sigma_T}{2}-2M_T \ , \tag{21}$$

where the total spin is

$$\sigma_T=\sum_{j=1}^{L}\sigma_j \ . \tag{22}$$

Notice that for $M_T=\sigma_T=0$, $S_T=3L/2$. It will turn out to be convenient to rewrite S_T in the form

$$S_T=\tfrac{3}{2}L-2\epsilon L \ . \tag{23}$$

For the PLL model, the value of ϵ is determined by our choice of S_T.

A. Solution of the periodic model

The conservation law for S_T in the periodic model will enable us to solve for the probabilities of the different values of M_T. Define the probability that the total trap number takes on a certain value, say M, in a system of size L as $\rho_T(M,L)$. This probability will certainly depend upon ϵ. Since S_T is conserved we can combine Eqs. (21) and (23) to read

$$\sigma_T=4(M_T-\epsilon L) \ . \tag{24}$$

Since the σ_j's fluctuate independently of one another, we know all about the statistical properties of variance of σ_T. From Eq. (24), we then know all about the statistical properties of M_T. Since each spin has average zero, the average trap number at a given site is

$$\sum_{M=1}^{\infty}\frac{\rho_T(M,L)M}{L}=\langle M_j\rangle=\epsilon \ . \tag{25}$$

We are interested in the case of small ϵ so that Eq. (25) can be interpreted as the statement that ϵ is the small probability that there will be a trap present at a site j. The existence of a nonzero ϵ in turn implies the existence of a typical length scale λ,

$$\lambda=\frac{1}{\epsilon} \ , \tag{26}$$

which is the mean distance between traps. The statistical independence of the different σ_j's means that we can calculate the variance of the total trap number from Eq. (24) as

$$\sum_{M=1}^{\infty}\rho_T(M,L)M^2=\langle(M_T-\epsilon L)^2\rangle=\frac{L}{16} \ . \tag{27}$$

The entire probability distribution of both σ_T and M_T can also be found quite easily. The independence of the σ_j's implies that the distribution for σ_T has a binomial character: For large L, the binomial distribution may be replaced by a Gaussian distribution. Since for the PLL model, the distributions of σ_T and M_T differ only by a constant, we know that the distribution of M_T is also Gaussian. Here the factors $8/L$ arise because the variance of $\langle\sigma_T^2\rangle$ is just L. Thus we find

$$\rho_T(M,L)=\frac{\exp[-8(M-\epsilon L)^2/L]}{\sqrt{\pi L/8}} \ . \tag{28}$$

Equation (28) is the central result of this section. It implies that the probability of observing values of the total trap number which are zero (or below) are of the order

$$\rho_T(0,L)=\exp[-8(-\epsilon L)^2/L] \ . \tag{29}$$

The exponential factor is the one which matters. The statement is that if

$$\frac{\epsilon^2 L}{\ln(L)}\gg 1 \ , \tag{30}$$

then there is an exponentially small probability that the system will have no traps. When the inequality (30) is sufficiently satisfied, the system will always contain many traps. If this model were a usual statistical-mechanical system, we would further expect that there was some coherence length ξ, which describes the typical size of these regions, and that over distances much greater than ξ, one could apply local equilibrium arguments to get estimates of probabilities. In particular, one could estimate the probability of finding a region of size x with a small value of $M(x)=\sum_{k=j}^{j+x}M_j$ by applying the analysis which led to Eq. (28). The result is

$$\rho_T(M,x)\sim\exp[-8(M-\epsilon x)^2/x] \ . \tag{31}$$

Notice that we have defined $\rho_T(M,x)$ to be the probability to see the total trap number M in a region of size x. Notice also that we have replaced an equality by an order of magnitude statement since the argument is unlikely to be sufficiently good to get the prefactor correctly. If we specialize to $M=0$, we find for the PLL model

$$\rho_T(0,x)\sim\exp(-8\epsilon^2 x) \quad \text{for } L>x\gg\xi\sqrt{\pi L/8} \ . \tag{32}$$

Equation (32) implies that there exists a second typical scale in this problem, ξ, which satisfies

$$\xi\sim\epsilon^{-2} \ . \tag{33}$$

This result may be in error by factors which behave as

powers of $\ln(L)$. However, it should be clear that for $x \gg \xi$ there is only an exponentially small probability to see no trap.

We now turn to the consideration of a smaller subsystem of the full system, and will try to introduce the effects of diffusion in an order of magnitude calculation. Assume an isolated system of size x, stretching from j to $j+x$. Corresponding to Eq. (21), but now over just the region of size x, the following relation holds:

$$S_T(x)=\frac{3}{2}x+\frac{\sigma_T(x)}{2}-2M_T(x) , \tag{34}$$

where the totals now represent sums over a region of size x. Start from an initial condition for which

$$M_T(x)\sim\epsilon x \tag{35}$$

and σ_T is roughly zero, where the region is large enough so that M_T is much larger than one, i.e.,

$$x \gg \epsilon^{-1} . \tag{36}$$

Consider a time interval t, which obeys $1 \ll t \ll L$. In this interval of order xt/L spins, σ_j will have flipped sign on the region. Correspondingly by the central limit theorem, the change in σ_T will be of the order

$$\delta\sigma_T(x)\sim\sqrt{xt/L} . \tag{37}$$

If one looks at a time interval larger than L, some of the spins that have flipped will start flipping back so that the fluctuations in σ_T will no longer grow, but remain fixed at the value of order $\sqrt{x}$. As $\sigma_T(x)$ changes, $4M_T(x)$ will change by the same amount, providing we neglect motion of traps in and out of the region. Therefore the time that it will take for a fluctuation to reduce the number of traps to zero will be $t^*(x)$, which is given by the time necessary for the fluctuation in $\sigma_T(x)$ to be of the order ϵx, i.e.,

$$xt^*(x)/L\sim(\epsilon x)^2 . \tag{38}$$

This estimate will be used in the context of the diffusion equation

$$\partial_t s_j \approx 2\partial_j\partial_j n_j . \tag{39}$$

Here s_j and n_j are coarse-grained versions of the slope S_j, and the local flip number n_j over a region much larger than the coherence length. Carlson, Chayes, Grannan, and Swindle (CCGS) [7,8] argued that a diffusion equation such as Eq. (39) would be necessarily satisfied by a coarse-grained slope and found numerical evidence for this diffusive behavior. We can see how this equation could arise. A coarse-grained averaging of Eq. (17) implied that in a typical avalanche step

$$s_j(t+\tfrac{1}{2})-s_j(t)=-4n_j+2n_{j+1}+2n_{j-1} , \tag{40}$$

so that the replacement of differences with derivatives gives Eq. (39). In deriving this estimate we have neglected changes in s_j caused by the direct addition process. We do this because any addition will raise one S_j at the expense of lowering the neighboring one. Thus direct additions tend to cancel out in the coarse graining of S_j. We use the scales already defined to estimate various quantities in Eq. (39), i.e., $\partial_j\sim x^{-1}$, $\partial_t\sim 1/[t^*(x)]$, $s_j\sim\epsilon$, and find

$$n_j\sim\frac{\epsilon x^2}{t^*(x)}\sim\frac{x}{\epsilon L} . \tag{41}$$

Next we estimate the number of grains that flow past each site in the system. To do so we must first define various probabilities and the relationship between them.

Define $Q(y)$ to be the average number of trap-free regions of size y in a system of large size L. Let $\rho_T(0,x)$ be the probability that a randomly picked region of size x will contain no traps whatsoever. Let $p(y)$ denote the probability that if you start out from any point j and move towards larger values of position you will encounter the first trap at $j+y$.

Notice that $p(y)L$ is the number of times you will land y steps to the right of the trap when one averages over all the possible entries. There will be one such entry of each trap-free region of size larger than y. Thus

$$p(y)L=\sum_{z=y}^{L}Q(z) . \tag{42}$$

Imagine that we pick a region by first specifying a random value of the starting point j and then walking to the left from that point. If there are no traps which appear as we walk over a distance x, we know that the region will make a contribution to $\rho_T(0,x)$. Thus

$$\rho_T(0,x)=\sum_{y=x}^{\infty}p(y) . \tag{43}$$

Next we would like to estimate the distributions for the drop numbers. To estimate $\rho_D(x)$, one notices that $p(x)$ is the probability that the first trap in the system will occur at a distance x from an arbitrarily chosen point. If one adds a grain at a distance $k<x$ from the trap, one will with probability $\frac{1}{4}$ (which is the asymptotic probability of seeing a pair of sites with $\epsilon_j=\epsilon_{j+1}=1$) start an avalanche. This will correspond to a drop number of $D=2(x-k)$. By this argument, one gets the drop number distribution function as

$$\rho_D(x)=\tfrac{1}{4}\sum_{y=x}^{L}p(y)/L . \tag{44}$$

To estimate $\langle N_j\rangle$, notice that the drop number in any avalanche is $2y$ so using Eq. (44)

$$\langle N_j\rangle=\sum_x 2x\rho_D(x)=\sum_0^L\frac{x}{2L}\sum_{y=x}^{L}p(y) . \tag{45}$$

Reversing the order of summation we get

$$\langle N_j\rangle=\sum_{y=0}^{L}\frac{y^2}{4L}p(y) . \tag{46}$$

At this point we note that the summation can be terminated at $y=\xi$ with impunity since $p(y)$ becomes exponentially small beyond this point. Thus to estimate n_j in Eq. (40) one uses

$$n_j \sim \sum_{y=0}^{x} \frac{y^2}{L} p(y) \tag{47}$$

to find that Eq. (41) implies

$$\sum_{y=0}^{x} \frac{y^2}{L} p(y) \sim \frac{x}{\epsilon L} . \tag{48}$$

Differentiating Eq. (48) this expression with respect to x, to find the estimate for the probability we get

$$p(x) \sim \frac{1}{\epsilon x^2} \quad \text{if } \epsilon^{-1} \ll x \lesssim \xi . \tag{49}$$

This is the central result of this section. The conditional in this equation arises from the two constraints in our calculation: first that x be large enough so that there are usually many traps in the region of size x, and second that x is small enough so that a sufficiently large fluctuation might occur. This will require that

$$x \lesssim \xi \sim \epsilon^{-2} . \tag{50}$$

The other limit in the conditional in Eq. (49) is the requirement that the size of the region be large compared to the typical distance between traps. We denote this typical distance by λ, where

$$\lambda = \epsilon^{-1} . \tag{51}$$

B. Predictions for the drop number

The scaling analysis of the preceding section can be employed to estimate the drop number distribution. First consider small values of x. Rewrite Eq. (44) as

$$\rho_D(x) = \frac{1}{4L} \left[1 - \sum_{y=0}^{x} p(y) \right] . \tag{52}$$

We have defined λ as the typical distance between traps. As such it should represent the x value for which the sum in Eq. (52) becomes of the order unity. As a result, when $x \ll \lambda$, ρ_D must become independent of x. We estimate

$$L\rho_D(x) \sim 1 \quad \text{for } 1 \ll x \ll \lambda . \tag{53}$$

We then use Eqs. (44) and (49) to get the drop number distribution in the scaling region as

$$L\rho_D(x) \sim \frac{1}{\epsilon x} \quad \text{for } \lambda \ll x < \xi . \tag{54}$$

Finally to obtain an estimate for large x, we employ Eqs. (43), (44), and (28) and find

$$L\rho_D(x) \sim \frac{\exp(-x/\xi)}{\sqrt{x}} \quad \text{for } \xi \ll x < L . \tag{55}$$

The numerical prefactor in the coherence length is defined so as to remove all the numerical prefactors from the exponent in Eq. (55) which then requires

$$\xi = \epsilon^{-2}/8 . \tag{56}$$

IV. THE LOCAL LIMITED MODEL REVISITED

In the LL model, the slope of the sandpile is no longer a conserved quantity. Thus Eq. (21) is no longer exact. However, numerical simulations show that the slope distribution is a sharply peaked quantity that is a function of the system size. The modal value of the slope obeys the following scaling relation

$$\langle S(L) \rangle - \tfrac{1}{2} \sim \epsilon \sim L^{-(1/3)} . \tag{57}$$

Thus one can expect our arguments for the PLL model to carry through to the LL model. However, in all of our arguments one must replace the free parameter ϵ with the observed value of $\epsilon(L)$.

Going back to Eq. (45), we now note that for the LL model $\langle N_1 \rangle = \frac{1}{2}$, since $\langle N_1 \rangle$ simply measures the number of pairs falling off from the first site, which by conservation is half the number of grains added. Apply Eq. (47) with the evaluation of $p(x) \sim p_0(x)$ given by Eq. (49). The contribution for x near the mean free path is quite small. The main contribution occurs for x of the order of the coherence length. We now find

$$\frac{\xi}{\epsilon L} \sim 1 , \tag{58}$$

which in conjunction with Eq. (50) enables us to evaluate ϵ and find

$$\epsilon \sim L^{-1/3} . \tag{59}$$

CCGS found the evaluation Eq. (59) as a result of their numerical work. This is a theoretical derivation. (A condensed version of this argument can be found in Ref. [9].) The above result can also be derived using a scaling argument which we now present. Referring back to the solution of Eq. (46), which is given by Eq. (49), we notice that one could in principle have other solutions of the form $p(y) = (L/\xi)(4/y^2)(\xi/y)^{\beta}$. We rule out such solutions by requiring that $\sum_{\lambda}^{\xi} p(y) \sim O(1)$. Then we use the fact that ϵ is the average probability to see a trap at any site and that $\lambda = 1/\epsilon$ defines a characteristic distance between traps. Therefore, for $1 < x < \lambda$ we get

$$\sum_{y=0}^{\lambda} p(y) \sim \int_0^{\lambda} \epsilon \exp(-\epsilon x) \sim 1 - 1/e . \tag{60}$$

Thus the probability of seeing a trap a distance greater than λ is of the order $1/e \sim O(1)$. Noting that $p(y)$ decays exponentially for $y > \xi$, we can write

$$\sum_{y=\lambda}^{\xi} p(y) \sim \frac{4L}{\xi} \left[\frac{1}{\lambda} - \frac{1}{\xi} \right] \sim O(1) . \tag{61}$$

Neglecting the term $1/\xi$ as small compared to $1/\lambda$ we get

$$\frac{L}{\xi \lambda^2} \sim \epsilon . \tag{62}$$

Using the relation $\lambda \sim \epsilon^{-1}$ we end up with

$$\frac{\xi}{4\epsilon L} \sim 1 , \tag{63}$$

which in conjunction with Eq. (33) enables us to evaluate ϵ

$$\epsilon \sim L^{-1/3} . \tag{64}$$

This immediately gives us expressions for the two fundamental length scales in the problem:

$$\lambda \sim \epsilon^{-1} \sim L^{1/3} \tag{65}$$

and

$$\xi \sim \epsilon^{-2} \sim L^{+2/3} . \tag{66}$$

The importance of this length scale with regard to the drop number distribution has also been emphasized in Ref. [10]. The drop number predictions for the PLL model given by Eqs. (53)–(55) also carry through, but with one important difference. Unlike the PLL model, L is no longer an irrelevant parameter but now sets the length scales for both ϵ and ξ.

Since the scaling relations all involve powers of L, the natural variable to use is the logarithm of L. We define multifractal like variables α and $G(\alpha)$, where

$$\alpha = \frac{\ln(x)}{\ln(L)} \tag{67}$$

and

$$G(\alpha) = \frac{\ln[\rho_D(x)]}{\ln(L)} . \tag{68}$$

Then combining Eqs. (53) and (54) with Eqs. (65) and (66) we get

$$G(\alpha) = -1 \quad \text{for } 0 < \alpha < \tfrac{1}{3} \tag{69}$$

and

$$G(\alpha) = -\tfrac{2}{3} - \alpha \quad \text{for } \tfrac{1}{3} < \alpha < \tfrac{2}{3} . \tag{70}$$

In the third region $\frac{2}{3} < \alpha < 1$ we expect an exponential falloff in the probability $\rho_D(x)$ and thus *asymptotically*

$$G(\alpha) = -\infty \quad \text{for } \tfrac{2}{3} < \alpha < 1 . \tag{71}$$

V. SIMULATIONS OF THE LL AND PLL MODELS

A. Simulations of the LL model

In this section, we will compare the theoretical predictions in the preceding sections with numerical evidence obtained via computer simulations of the LL model.

For very small lattice sizes, i.e., $L = 1-10$, one can calculate the eigenfunction of the Markov matrix of transitions and then compute the drop number distribution exactly. Since the number of recurrent configurations grows exponentially, for large L, it is impossible to carry through the calculation. Thus, for $L > 10$ we resorted to computer simulations. Due to the simple nature of the dynamics (as outlined in Sec. II B), one can write very efficient codes for updating the sandpile. In addition, one can estimate by various arguments that the transient time for the sandpile to reach its slope is of the order of L^2.

The theory predicts a scaling behavior based on two length scales, namely ϵ, which defines the characteristic distance between traps and $\xi \sim \epsilon^2$, a coherence length beyond which correlations decay exponentially. We show here two simple ways of estimating the L dependence of ϵ. Both of them are based on the idea that the L^2 sandpile has a slope distribution that is sharply peaked and that we can use the modal slope (i.e., the peak of the distribution) for all our scaling arguments.

Figure 4 is a log-lot plot of the deviation of the modal slope from its asymptotic value of 1.5. The slope of this plot [which from Eq. (23) is ϵ] is ~ 0.338. This is very close to the theoretical prediction of $\frac{1}{3}$.

Similarly one can look at the modal trap number distribution. Our theory predicts that deep traps are irrelevant and that the number of traps should scale like $\epsilon L \sim L^{2/3}$. Figure 5 is a log-log plot of the modal number of traps against lattice size. The slope of this plot gives us an estimate for ϵL. Its numerical value 0.688 is in good agreement with the theoretical prediction of $\frac{2}{3}$.

In the LL model, for each lattice size there is a distribution of slopes and trap numbers. The theory predicts a (truncated) Gaussian distribution for the trap numbers. Figures 6(a) and 6(b) show that this prediction is in good agreement with the observed trap number distribution.

For purposes of computing the above modal slopes and trap numbers, the sandpiles were updated about 10^8 times. For purposes of computing the statistics of drop numbers (avalanche sizes) we performed much larger simulations. This is necessary as the drop number distribution depends on the entire distribution of the trap numbers and not just the modal value.

For small lattice sizes, i.e., $L < 256$, we updated each sandpile 10^9 times. Since the probabilities of the drop numbers decrease as power laws or exponentials (depending on the scaling region) with lattice size, for lattice sizes $L > 256$ we employed the following trick to improve our

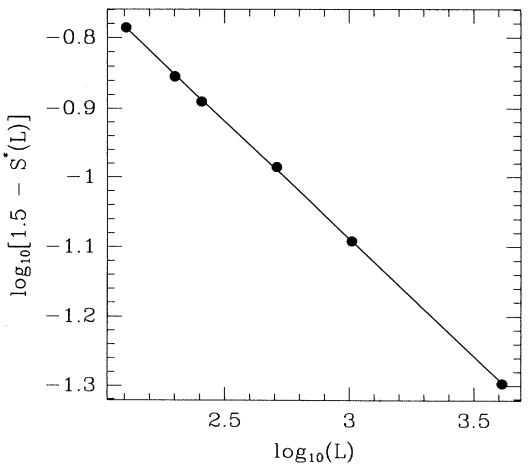

FIG. 4. Log-log plot of modal slopes. The sandpile has a sharply peaked slope distribution in time. The peak is a function of the system size and tends to $\frac{3}{2}$ in the thermodynamic limit. The theory predicts that the deviation from $\frac{3}{2}$ decreases as a power law in L with an exponent of $\frac{1}{3}$. The slope of the least-squares fit to the data points is 0.338.

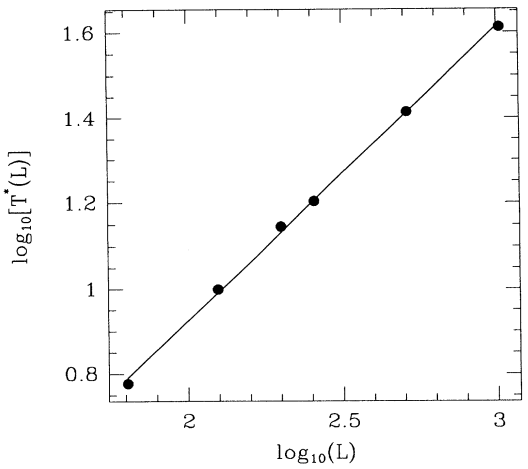

FIG. 5. Log plot of modal trap numbers. Similar to having an L-dependent modal slope (Fig. 4), the sandpile also has an L-dependent modal trap number. The theory predicts that the number of traps should increase as $L^{2/3}$. The slope of the least-squares fit to the data points is 0.688.

statistics. Notice that each site can receive a grain of sand with probability $1/L$. So we computed all the drop numbers that would have occurred if we dropped a grain of sand at each of the different possible sites of the sandpile. Then we chose a single site at random and updated the configuration. This enabled us to increase the number of events by a factor of L. For $256 \leq L \leq 50\,000$ we discarded the first L^2 transients and then gathered statistics while updating the sandpile 10^{10} times. These ($256 \leq L \leq 50\,000$) are our most extensive simulations and are several orders of magnitude more extensive than previous work in this area [1,7,8]. Nevertheless, they are not necessarily our most accurate simulations for all ranges of drop numbers. This is because the probability of various events decreases at least like a power law of the system size and therefore there is a tradeoff between increasing the system size to decrease finite-size effects and the number of updates required to get accurate simulations.

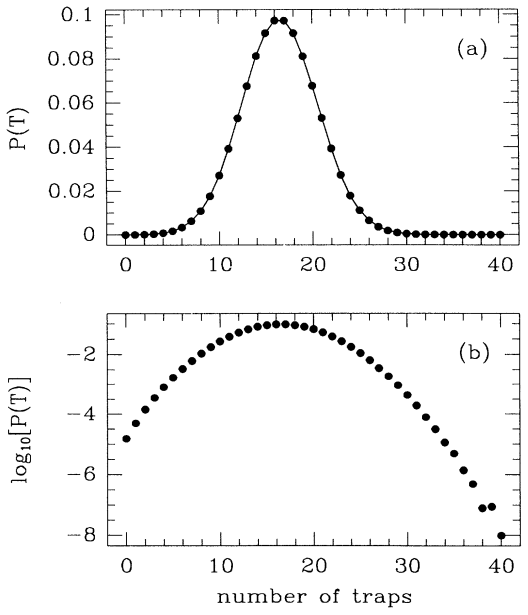

FIG. 6. Probability distribution of traps. The theory predicts that the fluctuations of trap numbers are gaussian in nature. These graphs provide support for such behavior.

The appropriate variable for the drop size in our scaling theory is $\alpha = \ln(D/2)/\ln(L)$. There are boundary effects in the LL model are at most a very slowly increasing function of L. Thus, if we use large lattice sizes, the boundary effects become negligible (i.e., restricted to very small values of α). For evaluation of small α values for some of the power-law plots we simulated much larger lattice sizes $10^5 < L < 10^6$. Since the transient times become prohibitively large, and the simulational time increases with L, for these lattice sizes we discarded less than L^2 transients (usually 2.5×10^9) and updated the lattice 10^9 times. In addition we used the previously described trick to increase the number of events by a factor of L.

For the drop number distribution the theory predicts a piecewise linear $G(\alpha)$ with three different kinds of scaling. Region I, $0 < \alpha < \frac{1}{3}$, $\rho_L(D/2)$ is expected to have an inverse L dependence [Eq. (53)]. Figures 7(a)–7(d) are log-log parts of $\rho_L(D/2)$ corresponding to four different α values in this region. Figure 7(a), which corresponds to $\alpha = \frac{1}{6}$, has a slope of -1.017, which is in good agreement with the theoretical prediction of a slope of -1. In fact, if one restricts oneself to large lattice sizes $5 \times 10^4 < L < 3 \times 10^5$, a least-squares fit yields a slope of -1.005. Figures 7(b) and 7(c) correspond to α values of $\frac{1}{5}$ and $\frac{1}{4}$, respectively. Both plots yield slopes of -1.004, which are in an excellent agreement with the theoretical prediction of -1. Figure 7(d) examines scaling at $\alpha = \frac{1}{3}$ and yields a slope -1.049, about 5% higher than predicted. This is the first of the two theoretically predicted phase transition points. Examining very large lattice sizes increases the slope to about 1.13. A possible reason for the larger discrepancy may be that one could be seeing the phase transition slightly before $\frac{1}{3}$ due to finite-size effects. This would then put us in the second region of scaling, where the slope is decreasing. Figure 7(e) is the corresponding log-log plot of $\rho_L(D/2)$ corresponding to $\alpha = \frac{1}{2}$. The theoretical prediction of $G = -1 - (\frac{1}{2} - \frac{1}{3}) = -\frac{7}{6} = -1.1666$ is reasonably close to the observed numerical value of -1.134.

The third region of scaling starts at $\alpha = \frac{2}{3}$. First, by a combination of conservation of mass and steepest-descent arguments one can show that the theoretical prediction for $G(\frac{2}{3})$ is $-\frac{4}{3}$. Figure 7(f) gives us a numerical value of -1.35, which is off by about 2%.

For the region $\alpha > \frac{2}{3}$, the theory [Eq. (55)] predicts an exponential decay in the probability of observing large drop numbers. Log-log plots of the drop probability at $\alpha = \frac{5}{6}$ [Fig. 7(g)] and $\alpha = 1$ [Fig. 7(h)] seem to show a slope which increases in magnitude with $\ln(L)$. Note that $\alpha = 1$ corresponds to the largest possible avalanche size, i.e., $D = 2L$.

Figure 8 compares theory and numerics for the entire

$G(\alpha)$ curve. As we have shown before, there are small discrepancies of up to 5% between the theory and simulations.

We now look at finite-size plots of the avalanche data, attempting to check the more detailed predictions of Eqs. (53)–(55). Equation (53) tells us the scaling of $\rho(D)\sim 1/L$ for $0<\alpha<\frac{1}{3}$. This is seen quite well in the plots in Figs. 7(a) and 7(b). There is some discrepancy in the small α region which is due to a boundary effect. Consistent with this interpretation, we have seen that the

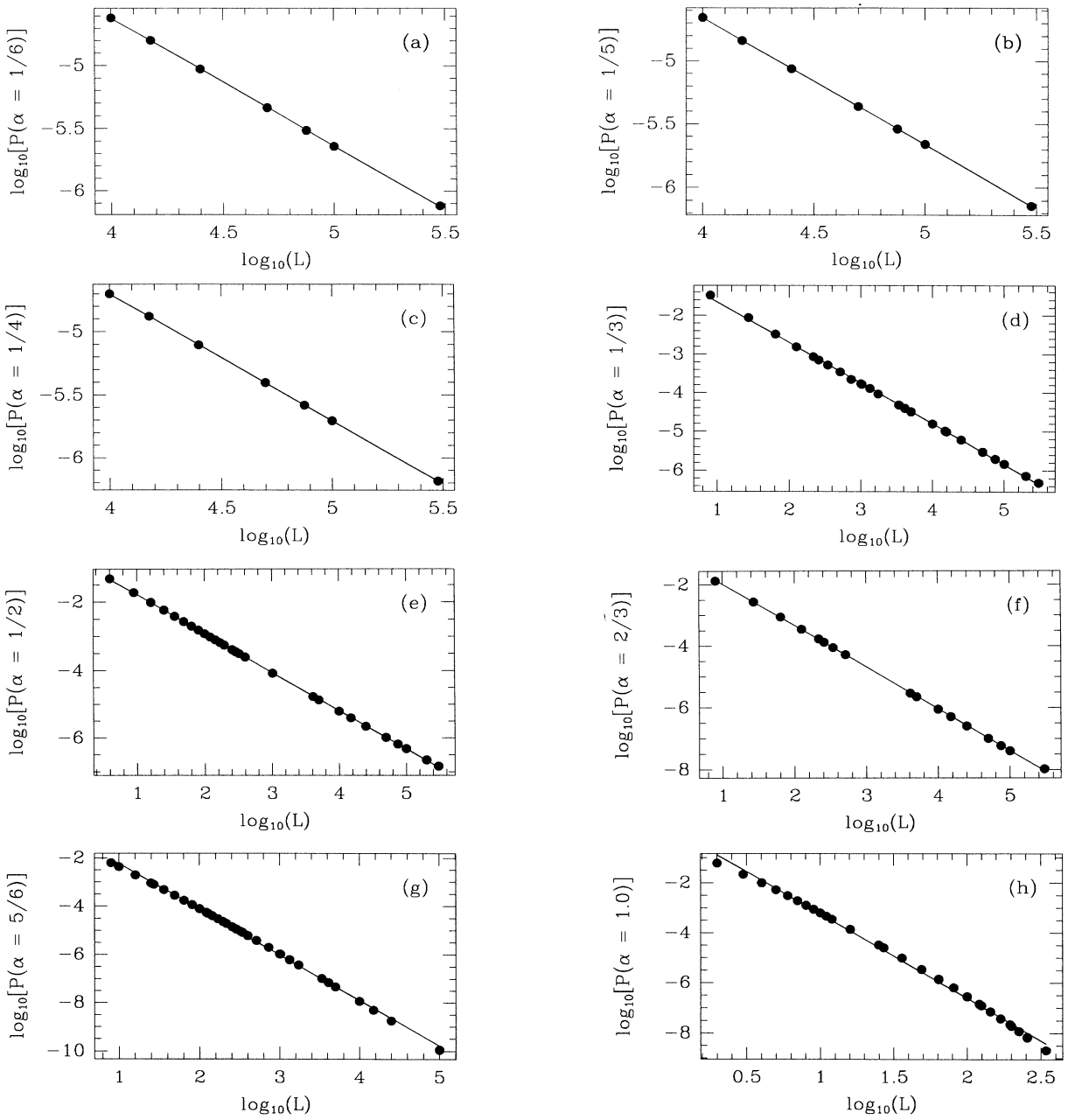

FIG. 7. Log-log plots of $\rho_L(D/2)$ for (a) $\alpha=\frac{1}{6}$ and (b) $\alpha=\frac{1}{5}$ (region I). The theoretical prediction for the slopes is -1. The slopes of the least-squares fit to the data points are -1.017 and -1.005, respectively. Very large lattice sizes $50\,000<L<300\,000$ (not shown here) yield slopes of -1.005 and -1.002, respectively. Log-log plots of $\rho_L(D/2)$ for (c) $\alpha=\frac{1}{4}$ and (d) $\alpha=\frac{1}{3}$ (region I). The theoretical prediction for the slopes is -1. The slopes of the least-squares fit to the data points are -1.004 and -1.049, respectively. Very large lattice sizes $50\,000<L<300\,000$ (not shown here) yield slopes of -1.004 and -1.13, respectively. Log-log plots of $\rho_L(D/2)$ for (e) $\alpha=\frac{1}{2}$ and (f) $\alpha=\frac{2}{3}$ (region II). The theoretical prediction for the slopes is $G(\frac{1}{2})=-\frac{7}{6}=-1.166$ and $G(\frac{2}{3})=-\frac{4}{3}=-1.333$. The slopes of the least-squares fit to the data points are -1.135 and -1.351, respectively. Log-log plots of $\rho_L(D/2)$ for (g) $\alpha=\frac{5}{6}$ and (h) $\alpha=1$ (region III). These plots [(g) and (h)] in contrast to the ones at lower α values show a faster-than-power-law decay, consistent with the theory which predicts an exponential falloff.

agreement in this region gets better as we go to larger lattice sizes, where the boundary effect is negligible. Equation (54) tells us that $\epsilon L x \rho(x) \sim$ const. Figure 9 shows such a finite-size scaling plot. There does not appear to be any satisfactory convergence to a horizontal plateau with increasing L. Figure 10 shows the same plot, but plotted against α. Since we estimate $\epsilon \sim L^{-1/3}$, this means that we expect $L^{2/3}(D/2)\rho(D/2) \sim$ const. for $\frac{1}{3} < \alpha < \frac{2}{3}$. Although there is a clear signal of a change in scaling behavior in the region around $\frac{1}{3}$ and then again around $\frac{2}{3}$, it is clear that the function is not constant in this region. Instead, as L gets larger, the function gets steeper. Thus clearly we have not eliminated the L dependence from these plots. To understand whether these are finite-size effects or whether the theory has additional scales that we have not taken into account, we attempt to determine whether the deviations shown are exponentially small corrections in L (permitted by the theory) or rather power-law corrections in L, which then would have to be incorporated in the theory. We do this by first estimating the exponential function in region III and then incorporating this correction on our data for region II. To check the exponential fall off in region III ($\frac{1}{3} < \alpha < \frac{2}{3}$), in Fig. 11 we plot the same function as in Fig. 10, but now against the variable $x/L^{2/3}$. The data are consistent with an exponential falloff, though there is some upturn in the tails for large L. From Fig. 11 we estimate the exponent of the exponential to be about $\frac{7}{20}$. We now correct for this exponential factor in region II,

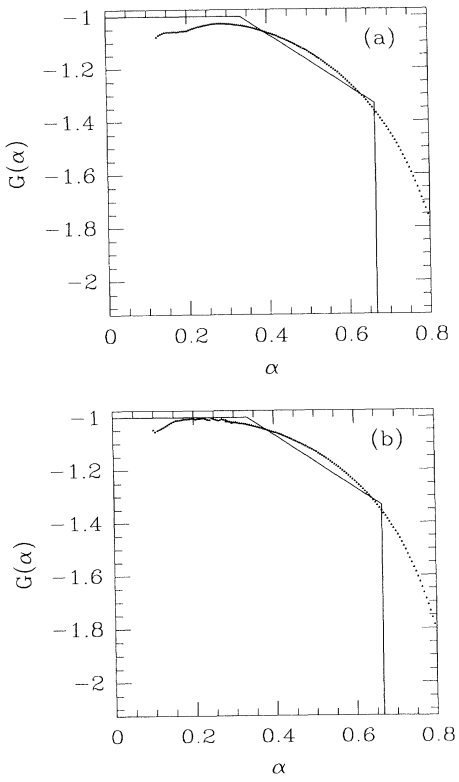

FIG. 8. Entire $G(\alpha)$ plot. Assuming a multifractal scaling. The solid line is the theoretical prediction. The region beyond $\alpha = \frac{2}{3}$ needs careful interpretation. The reader is urged to look at Figs. 7(e) and 7(f) carefully to judge the validity of the claim that the exponents in this region are a result of fitting a power law through a finite range of data which are in fact actually falling off (very slowly) faster than a power law. (b) was obtained by using very large lattice sizes $10^4 < L < 10^5$ to compute $G(\alpha)$ for small α values and interpolating this curve with the function shown in (a).

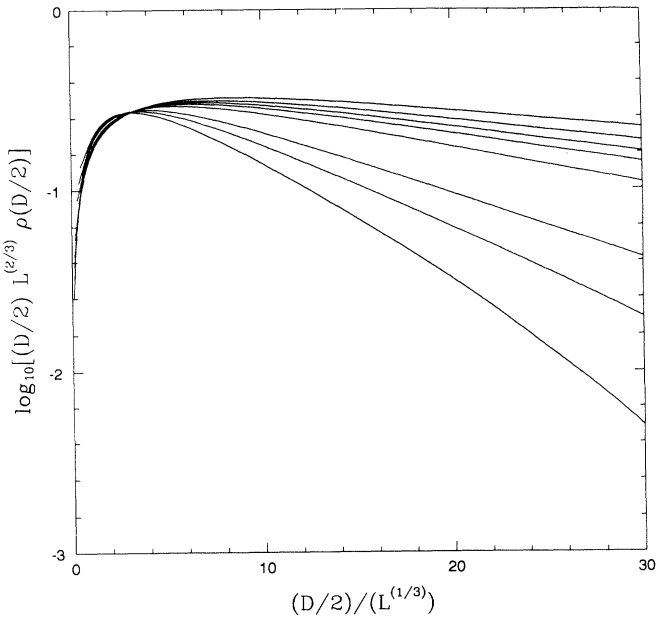

FIG. 9. Finite-size scaling plot for region II, i.e., $\frac{1}{3} < \alpha < \frac{2}{3}$. Shown are data from lattice sizes $L = 256, 512, 1024, 5\times10^3, 10\times10^3, 15\times10^3, 25\times10^3, 50\times10^3$, each set averaged over 10^{10} additions of sand. The abscissa is the avalanche size normalized by the mean trap distance. The ordinate is the logarithm of $\epsilon L D/2$, which the theory predicts should be a constant in the region $\lambda < D/2 < \xi$.

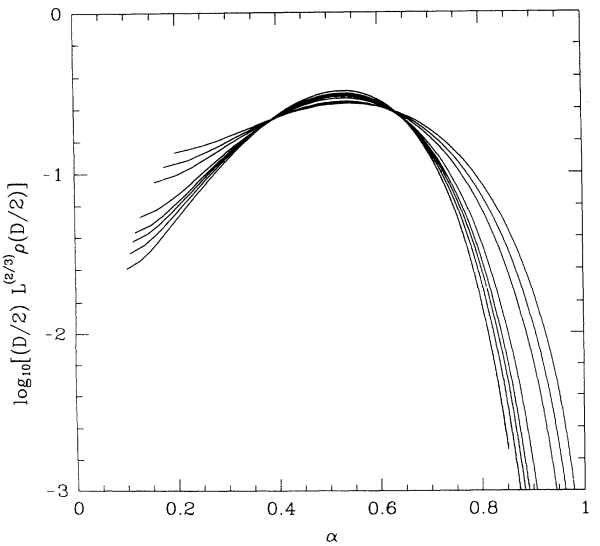

FIG. 10. The same quantity as in Fig. 9, but now plotted against α. The theory predicts a plateau in the region $\frac{1}{3} < \alpha < \frac{2}{3}$. The curves in this region, however, get steeper as L increases.

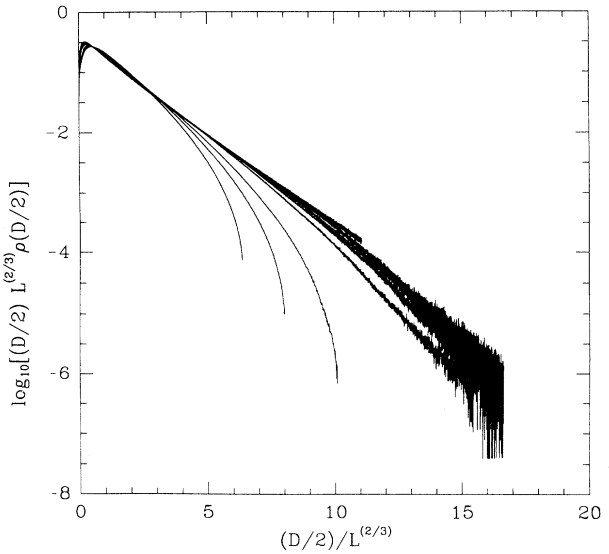

FIG. 11. Finite-size scaling plot for region III, i.e., $\frac{1}{3}<\alpha<\frac{2}{3}$. The ordinate is the logarithm of $\epsilon LD/2$. The theory predicts that there should be an exponential falloff in this region, as seen in the figure. However, notice that as one goes to larger lattice sizes there is a small tendency for the curve to move upwards. It is not known if this is an effect due to bad statistics (not equilibrating the system long enough) or a systematic effect not addressed by the theory.

and plot $\ln[L^{2/3}(D/2)\rho(D/2)\exp(aD/2L^{2/3})]$ vs α (where $a=\frac{7}{20}$) in Fig. 12. This figure shows considerable improvement compared to Fig. 10. However, the fact that the curves do not all collapse onto a single universal

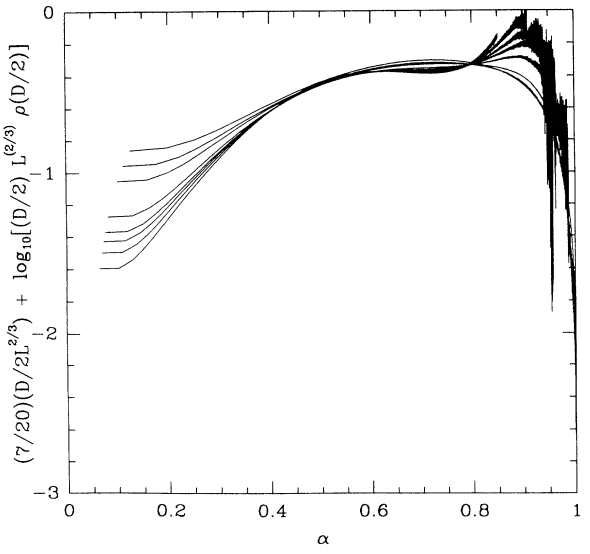

FIG. 12. Identical to Fig. 10, but now with an exponential correction (determined from the slope in Fig. 11) incorporated. Note the improvement of the expected plateau in the region $\frac{1}{2}<\alpha<\frac{2}{3}$. It is difficult to determine whether the observed discrepancy between theory and experiment is a result of such exponential corrections or a result of additional unknown length scales.

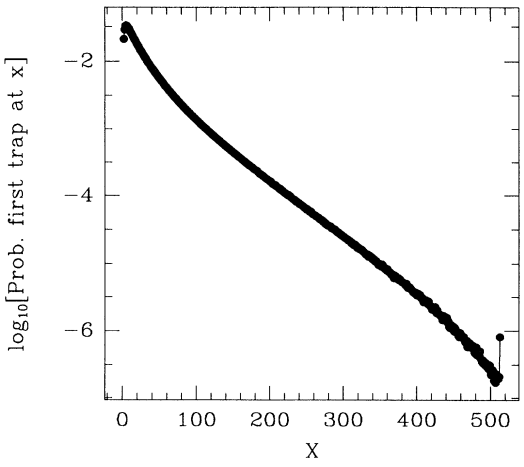

FIG. 13. Probability that the first trap will be at a distance y from the abyss for the LL model with $L=512$.

curve in the region $\frac{1}{3}<\alpha<\frac{2}{3}$ and that the function for the larger lattice sizes systematically moves downwards in this region implies that more corrections or prefactors may need to be incorporated before satisfactory collapse is obtained.

It is crucial to try and understand whether these discrepancies are due to finite-size and boundary effects in an inhomogeneous system or to the presence of other length scales not considered by the theory. We have seen in this section that the theory based on two length scales seems to predict the scaling behavior of the LL model to within a few percent. It is not clear whether we should expect better, since we are dealing with an inhomogeneous system because of the nature of the (one open, one closed) boundary conditions.

A quantity of interest is the probability distribution $p_0(y)$, which is the probability that the first trap will be at a distance y from the abyss. Figure 13 plots this quantity for $L=256$. Note the presence of boundary effects on both sides. As a check to some of the assumptions, particularly the assumption that neighboring sites of slope ($\epsilon_j=\epsilon_{j+1}=1$) occur (asymptotically) with probability $\frac{1}{4}$, one can compare the computed drop number distribution with the drop number distribution derived from $p_0(y)$ using Eq. (44). Figure 14 shows that there is fairly good agreement between these quantities. The small discrepancy may be caused by the fact that the probability of $\epsilon_j=\epsilon_{j+1}=1$ is actually slightly less than $\frac{1}{4}$ due to the presence of traps.

In the next section we will present a detailed simulational study of the PLL model and compare the results with the theoretical predictions made here. The hope is that the scaling of the data will be cleaner due to the translational invariance of the model.

B. Simulations of the PLL model

The PLL model has the advantage of being translationally invariant, but now we have a two parameter scaling. In the LL model, ϵ was a function of L. Here it is an independent conserved parameter whose value we can

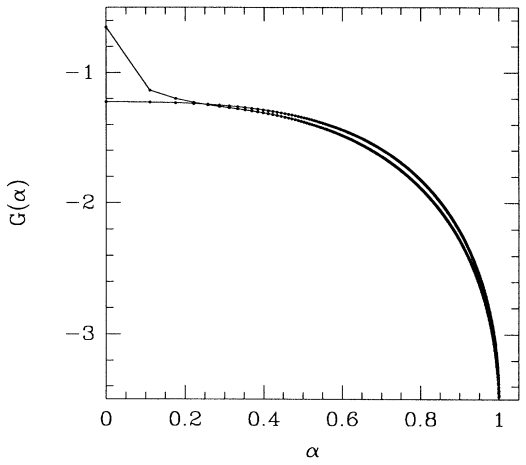

FIG. 14. Comparison between the actual drop number probability and that derived from the previous plot (LL model).

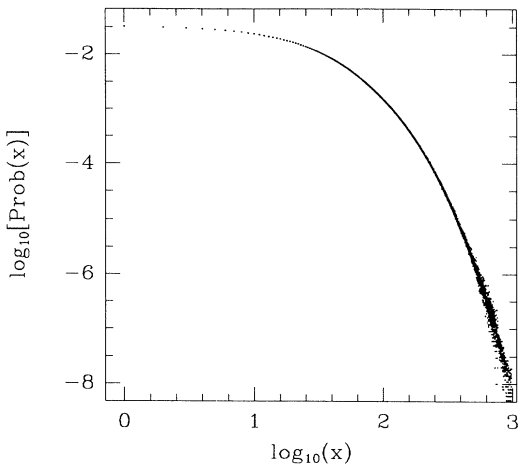

FIG. 16. Log-log plot of Prob(x) vs x for slope $=1.44$. L ranges from 4096 to 25 000.

choose. L, on the other hand, is now an irrelevant variable, which enters in the scaling theory as ϵ^{-3}. One must be sure to choose a large enough lattice size so that the system never "feels" its periodicity. The latter would happen if the number of traps in the system gets small. Thus one must choose L large enough so that one always has many traps in the system. Naturally this value of L is a function of both ϵ and the number of time steps considered. In particular one has work with larger and larger system sizes as $\epsilon \to 0$ and as $t \to \infty$.

Before examining the scaling of the PLL model let us fix a few definitions. Since the flow of sand is clockwise, we will call anything to the right of the site where sand was just added as the forward direction and to the left the backward direction. Then denote Prob(x) as the probability of the first trap being at a distance x behind a site from which sand was just added.

Figure 15 shows a log-log plot of Prob(x) for a variety of different system sizes all at a slope of 1.4. The lattice sizes range from 256 to 15 625. We see that all of the data except for $L=256$ and to a lesser degree $L=512$ collapse nicely. The lack of data collapse for $L=256$ can be explained by noting that an ϵ of 1.4 corresponds to a system size of about 512 in the LL model. Thus $L=256$ is too small a lattice size and the system "feels" its finiteness. Figure 16 plots the same quantities as Fig. 15, but now for $\epsilon=1.44$. These plots confirm that we are using large enough lattice sizes for our simulations and that the minimum lattice size increases as $\epsilon \to 0$.

In order to make a direct comparison with the LL model, we simulated the PLL model for different values of L and their corresponding ϵ, which were chosen to be equal to the modal ϵ that the LL model would have at that value of L. [We remind the reader that, in the LL model, $\epsilon=(S-1.5)/2$ is a fluctuating quantity since the slope is not a conserved quantity. It is, however, a sharply peaked distribution whose modal values we have used to define an ϵ for the LL model.] For these sets of simulations, we should thus be able to plot our data both

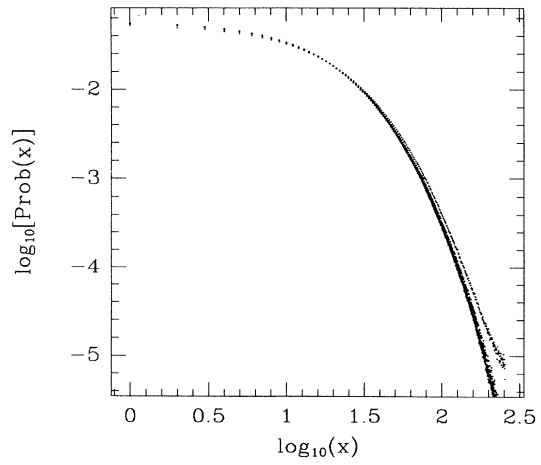

FIG. 15. Log-log plot of Prob(x) vs x for slope $=1.4$. L ranges from 256 to 15 625.

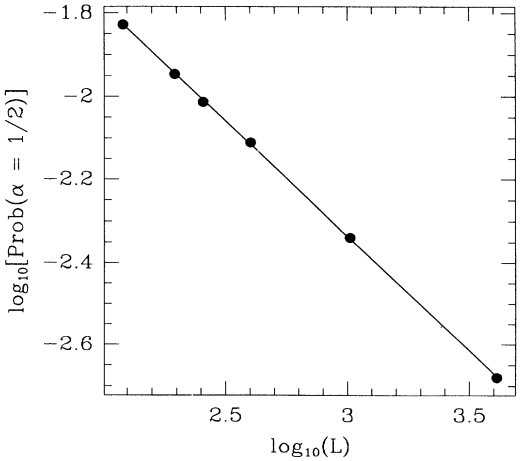

FIG. 17. Log-log plot of Prob($x=\sqrt{L}$) vs $\log_{10}(L)$, PLL simulation using different L's with ϵ's chosen to match the corresponding ϵ in the LL model.

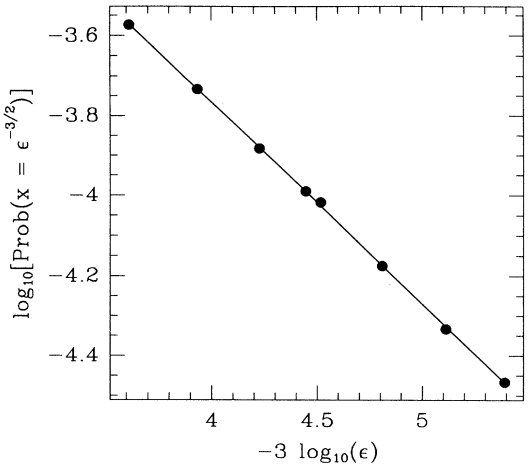

FIG. 18. Identical to Fig. 17, but with Prob($x=\epsilon^{-3/2}$) plotted against $-3.0\log_{10}\epsilon$.

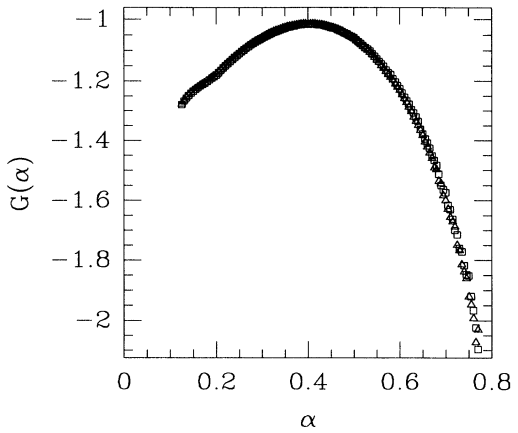

FIG. 20. Comparison between the $G(\alpha)$ for the PLL model with ϵ's corresponding to the LL model, where the scaling was done both against $\log_{10}(L)$ and $[2.5\log_{10}(\epsilon)]^{-3/2}$.

against $\ln(L)$ or against $\ln(\epsilon)$ and get the same numbers. As a first check we plot log-log plots of the probability of Prob($x=L^{1/2}$), which estimates drops of size $\alpha=0.5$. Figure 17 yields a slope of 0.59. If now we choose an ϵ based definition of α (i.e., using the relation $L\sim\epsilon^{-3}$), and plot Prob($x=\epsilon^{-3/2}$), we find that the quality of the log-log plot (Fig. 18) is not very good and the exponent is 0.55, i.e., about 10% off the value obtained from the L based definition of α. The reason for this is that, in our PLL models, we define ϵ as $(S-S_c)/2$, where $S_c=1.5$ and S is the slope of the PLL model. However, to get an explicit link between L and ϵ in order to compare the PLL and LL models, we have to worry about prefactors. The simplest assumption to make is $\epsilon=AL^{-1/3}$, where the prefactor A can be estimated in several ways. Two of them are, from the modal total number of traps in the LL model where to a very good approximation $M_T=2\epsilon L$, and from the deviation of the modal slope of the LL model from 1.5, which to a good approximation goes as ϵ. The factor A can be estimated from the intercept of both these plots and is found to be about 0.4 with an error of about 5%. Thus, when we compare a PLL simulation with a LL simulation, we should multiply the value of ϵ used in our scaling plots by a factor of $1/A=2.5$. As a check, we will show that this value of the prefactor also turns out to be the best value that makes the PLL data collapse for arbitrary values of L and ϵ.

Now, putting in the above discussed prefactor (A) in the definition of ϵ, and plotting Prob$[x=(2.5\epsilon)^{-3/2}]$ we find, as shown in Fig. 19, that not only do we now have a better log-log fit, but both the raw numbers and the exponent (0.59) are in agreement with those obtained from the simulations of the LL model.

The above scaling plots showing power-law scaling are similar to those observed in the LL model. We therefore follow the same procedure of finding the prefactor function $A(\alpha)$ by considering log-log plots, at various values of α and measuring the intercept. After eliminating this prefactor function, we plot the $G(\alpha)$ curves corresponding to both scaling with $\ln(L)$ and $(2.5\epsilon)^{-3/2}$ in Fig. 20. The excellent agreement over all ranges of α are an indication that the prefactor $1/A=2.5$ is indeed the correct

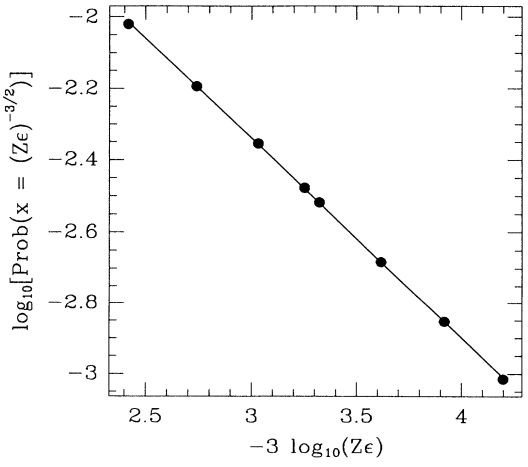

FIG. 19. Identical to Fig. 18, but all values of ϵ have been multiplied by $1/A=2.5$.

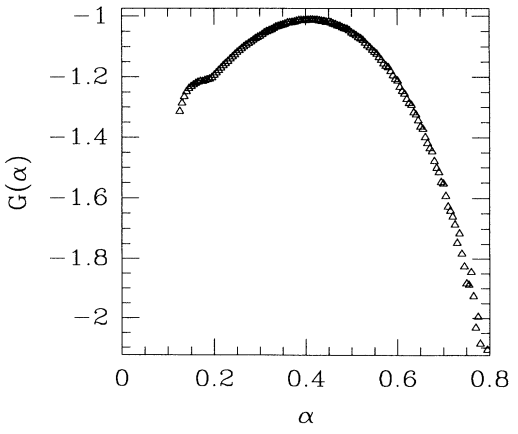

FIG. 21. $G(\alpha)$ for the PLL model with $L=15\,625$ with ϵ's that have been varied systematically from 0.06 to 0.01.

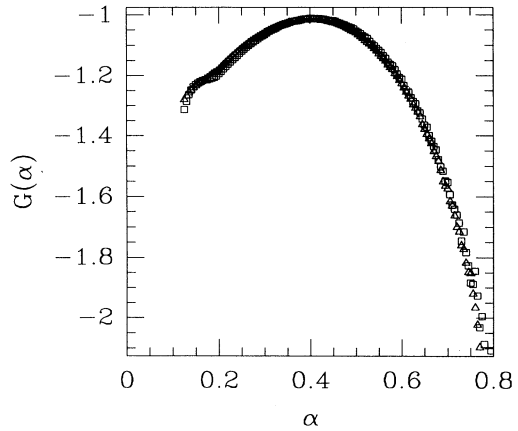

FIG. 22. Comparison between the $G(\alpha)$ for the PLL model with ϵ's corresponding to the LL model, and for runs with arbitrary values of ϵ with $L=15\,625$.

choice.

If our scaling relations are correct, then we should be able to collapse the PLL simulations for arbitrary ϵ (simulated on an appropriate large enough L), and not just for simulations where ϵ is chosen to correspond to the LL model. We choose a moderately large lattice size $L=15\,625$ and simulate the PLL model for a variety of ϵ values ranging from 0.06 to 0.01, which correspond to slopes ranging from 1.38 to 1.48. Once again, we assume power-law scaling, eliminate the prefactor function and multiply ϵ by the factor $A=2.5$. The result is a nice data collapse as shown in Fig. 21.

In Fig. 22 we show a comparison between the $G(\alpha)$ function from the set of runs with different L's and their corresponding ϵ's chosen from the LL model and those from the runs where L was kept constant and ϵ was varied systematically. The nice agreement clearly shows that we have captured the correct relation between ϵ and L. In Fig. 23 we compare this $G(\alpha)$ curve with the theoretical prediction. Here we see that once again the theory seems to have captured several of the essential types of behavior; in some cases however, it is as much as 15% off in its values.

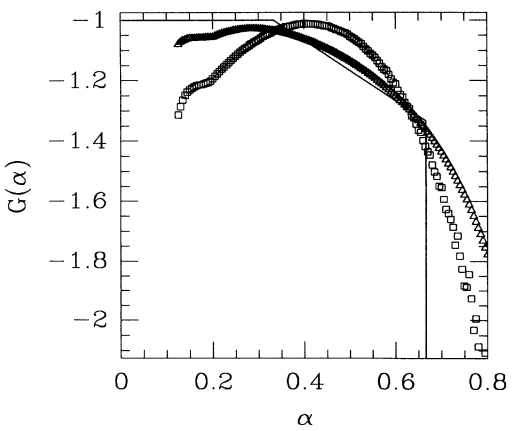

FIG. 23. $G(\alpha)$ comparison between theory and PLL simulations and LL simulations.

VI. LIMITED TRAP MODELS

To get further insight into the scaling behavior of this slope-dependent class of sandpile models, we consider a variant, the LLL model. In this model, the rules of evolution are similar to the LL model, however, traps are not allowed to form. Thus any avalanche, once started, backpropagates all the way to the wall. The main qualitative result is that in this case the system becomes correlated over its entire extent. This property is very different from the LL model, where the traps introduce a correlation length which is much shorter than the size of the system. Nevertheless, the model turns out to have extremely interesting properties that are strangely reminiscent of fluid dynamical problems. Capturing the essentials of a genuine transport problem, a diffusion equation appears naturally in terms of the slope variable. We will show that the LLL model can be solved in the mean-field approximation that is very similar to the standard closure approximation in fluid mechanics.

Rules for the LLL model

Recall the definition of ϵ_i, which is given by

$$\epsilon_i = H_{i+1} - H_i - 1 = S_i - 1 \ . \tag{72}$$

The time evolution of the model consists of randomly choosing a site and adding a grain of sand, subject to the following rules and constraints.

(R1) ϵ_i can only take on two values 0 or 1. The boundary condition is given by $\epsilon_{L+1}=1$.

(R2) It is illegal to add on site i when $\epsilon_i=\epsilon_{i+1}=0$.

(R3) If $\epsilon_i=0$ and $\epsilon_{i+1}=1$, then addition on site i will result in $\epsilon_i=1$ and $\epsilon_{i+1}=0$. There is no movement of sand in this case and therefore no avalanches.

(R4) If $\epsilon_i=1$ and $\epsilon_{i+1}=0$, then addition on site i will result in $\epsilon_i=0$ and $\epsilon_{i+1}=1$. A trivial avalanche of size 1 is created and a pair of sand grains fall into the abyss.

(R5) If $\epsilon_i=\epsilon_{i+1}=1$, then addition on site i will result in both the values being set to 0 as well as an avalanche of size $L-i+1$.

These rules completely describe the model. The reader is urged to check that these rules are identical to those of the LL model, except that the creation of traps is not allowed, so all backavalanches, once started, propagate all the way back to the wall and then slide off into the abyss.

Recall that to generate a backavalanche in the LL model one needed to add on a site with slope 2 and whose left neighbor also had a local slope of 2. This generated a backavalanche of a specified size which was determined by the proximity of the nearest (left-hand) trap.

It is then apparent that backavalanches are caused by the addition of a grain of sand on site i where $\epsilon_i=\epsilon_{i+1}=1$. The entire complexity of the avalanche sizes for avalanches bigger than 2 depends on the probability of adding on a 11 pair. Once we can compute the probability distribution of this quantity, it is trivial to compute the drop number distribution.

Before beginning our formal manipulations, let us note that rule (R2) makes this model significantly different from the previous two models we have analyzed. In

those cases the probability of choosing a site for addition was uniformly L^{-1} and independent of the configuration of the pile. In this model there is a new nonlinearity in that the probability of an addition site, while uniform over allowed sites, is now K^{-1} (configuration) with K, the number of available sites, decidedly dependent upon the momentary configuration. One of the consequences of this property is that while the probability to see a drop of size $L+1-i$, $i>1$ is the probability of $\epsilon_i=\epsilon_{i+1}=1$, it is of course really that probability weighted by the probability of selecting site i, which is now configuration dependent:

$$\text{Prob}(d=L+1-i)=\sum_{\{\epsilon\}} p_{\epsilon_1\cdots\epsilon_i\cdots\epsilon_L}\,\epsilon_i\epsilon_{i+1}K^{-1}(\epsilon_1\cdots\epsilon_i\cdots\epsilon_L)\ , \tag{73}$$

where $P_{\epsilon_1\cdots\epsilon_i\cdots\epsilon_L}$ is the true invariant probability distribution for the above process where each addition is an allowed process. K^{-1} is a major nuisance, but intuitively should be no more than a nuisance, since intuitively one can inflate the number of trials of the addition process by now selecting sites with probability L^{-1}, but simply doing nothing if an illegal addition is selected. (Really nothing, a grain is not even added.) It is important to make this precise. (The intuition is really right only when the process reaches its invariant distribution.) To do this, let us write out the details of the Markov process more formally. Denote by $|\epsilon_1\cdots\epsilon_i\cdots\epsilon_L\rangle$ a given configuration of the system. Define the diagonal operator K to be the count of the available sites:

$$K|\epsilon_1\cdots\epsilon_i\cdots\epsilon_L\rangle \equiv K(\epsilon_1\cdots\epsilon_i\cdots\epsilon_L)|\epsilon_1\cdots\epsilon_i\cdots\epsilon_L\rangle\ . \tag{74}$$

Write the momentary distribution function of the configurational probabilities as the vector p,

$$p=\sum_{\{\epsilon\}} p_{\epsilon_1\cdots\epsilon_i\cdots\epsilon_L}|\epsilon_1\cdots\epsilon_i\cdots\epsilon_L\rangle\ , \tag{75}$$

and define $\tilde{T}$ as the transition operator that sends $|\epsilon_1\cdots\epsilon_i\cdots\epsilon_L\rangle$ into the sum of all the states, each arising from the addition to an allowed site. Equipped with the inner product,

$$\langle\epsilon_1'\cdots\epsilon_i'\cdots\epsilon_L'|\epsilon_1\cdots\epsilon_i\cdots\epsilon_L\rangle=\prod\delta_{\epsilon_i',\epsilon_i}\ . \tag{76}$$

Then

$$\langle\epsilon_1'\cdots\epsilon_i'\cdots\epsilon_L'|\tilde{T}|\epsilon_1\cdots\epsilon_i\cdots\epsilon_L\rangle=1\ , \tag{77}$$

if a legal addition can produce $|\epsilon_1'\cdots\epsilon_i'\cdots\epsilon_L'\rangle$. Our process is now described by probability conservation as

$$p'=\tilde{T}K^{-1}p\ . \tag{78}$$

It is now easy to get rid of the K^{-1}. Namely, define a transformed probability π which absorbs the K^{-1}:

$$K^{-1}p=k^{-1}\pi\ , \tag{79}$$

where k is the number that normalizes π to a probability

$$k^{-1}=\sum_{\{\epsilon\}}\frac{1}{K(\epsilon_1\cdots\epsilon_i\cdots\epsilon_L)}p_{\epsilon_1\cdots\epsilon_i\cdots\epsilon_L} \tag{80}$$

and depends upon the distribution p. Dynamically, by (78) and (79) we have

$$k'^{-1}\pi'=K^{-1}p'=K^{-1}\tilde{T}(K^{-1}p)=k^{-1}K^{-1}\tilde{T}\pi \tag{81}$$

and

$$k'^{-1}=k^{-1}\sum_{\{\epsilon\}}\langle\epsilon_1\cdots\epsilon_i\cdots\epsilon_L|K^{-1}\tilde{T}\pi\ . \tag{82}$$

The π process is exactly equivalent to that of p. Notice that the *invariant* π distribution $\pi'=\pi$ satisfies

$$\pi=K^{-1}\tilde{T}\pi \tag{83}$$

or

$$K\pi=\tilde{T}\pi \tag{84}$$

so that the need to invert K is eliminated for this purpose. Next write

$$K=L\mathbb{1}-F \tag{85}$$

where $\mathbb{1}$ is the identity and F counts the forbidden addition sites. Then (84) becomes

$$\pi=L^{-1}(F+\tilde{T})\pi\ . \tag{86}$$

Equation (86) unearths the intuitive do-nothing process, F and $\tilde{T}$ always produce L new configurations, although F produces exact copies of the original (the do-nothing part), and each choice has uniform probability L^{-1}. Indeed, it can be verified that

$$\pi'=L^{-1}(F+\tilde{T})\pi \tag{87}$$

is Markov (i.e., probabilities are conserved), and is exactly the intuitive inflated process. It is *not* equivalent to (81) or (78): rather it has exactly the same invariant distribution as (81), which by (79) determines that of the original process (78). It should be clear that (87) does not easily relate to (78) out of stationarity. It is only when the rate of abortive additions is constant that they can be interconnected. Towards this end (79) is rearranged and summed to produce

$$k=\sum_{\epsilon}\pi_{\epsilon_1\cdots\epsilon_i\cdots\epsilon_L}K(\epsilon_1\cdots\epsilon_i\cdots\epsilon_L)\ . \tag{88}$$

We have produced (86) for good reasons. First (86) eliminates the inverse of K and so it is simple to write down explicitly in an easy manipulable form. Second, our desired drop distribution function (73) now becomes trivial. Equation (88) projected on $\langle\epsilon_1\cdots\epsilon_i\cdots\epsilon_L|$ reads

$$K^{-1}(\epsilon_1\cdots\epsilon_i\cdots\epsilon_L)p_{\epsilon_1\cdots\epsilon_i\cdots\epsilon_L}=k^{-1}\pi_{\epsilon_1\cdots\epsilon_i\cdots\epsilon_L} \tag{89}$$

so that (1) is now

$$\text{Prob}(d=L+1-i)=k^{-1}\sum_{\{\epsilon\}}\pi_{\epsilon_1\cdots\epsilon_i\cdots\epsilon_L}\epsilon_i\epsilon_{i+1} =k^{-1}\langle\epsilon_i\epsilon_{i+1}\rangle_\pi \tag{90}$$

Thus, with k given by (88), it is precisely the π invariant distribution of (86) that we wanted.

Finally, let us explicitly write down the operators $K, F, \tilde{T}$. Define the projection operator Z_i by

$$Z_i|\epsilon_1 \cdots \epsilon_i \cdots \epsilon_L\rangle = \bar{\epsilon}_i|\epsilon_1 \cdots \epsilon_i \cdots \epsilon_L\rangle \ , \tag{91}$$

where $\bar{\epsilon}=1-\epsilon$ is the binary conjugate of ϵ. Then

$$F=\sum_1^{L-1} Z_i Z_{i+1} \ . \tag{92}$$

$\tilde{T}$ projects out non-00 sites and then flips them:

$$\tilde{T}=\sum_1^{L-1} \sigma_i \sigma_{i+1}(1-Z_i Z_{i+1})+\sigma_L \ , \tag{93}$$

where σ_i is the flip

$$\sigma_i|\epsilon_1 \cdots \epsilon_i \cdots \epsilon_L\rangle = |\epsilon_1 \cdots \bar{\epsilon}_i \cdots \epsilon_L\rangle \ . \tag{94}$$

Substituting in (86) and projecting upon $\langle \epsilon_1 \cdots \epsilon_i \cdots \epsilon_L|$ produces a master equation that expresses the fact that in equilibrium, the change of probability of any configuration is zero:

$$\pi_{\epsilon_1 \cdots \epsilon_i \cdots \epsilon_L} + \sum_1^{L-1} (1-\bar{\epsilon}_1 \bar{\epsilon}_{i+1}) \pi_{\epsilon_1 \cdots \epsilon_i \cdots \epsilon_L} = \sum_1^{L-1} (1-\epsilon_i \epsilon_{i+1}) \pi_{\epsilon_1 \cdots \bar{\epsilon}_i \epsilon_{i+1} \cdots \epsilon_L} + \pi_{\epsilon_1 \cdots \epsilon_i, \epsilon_{i+1} \cdots \bar{\epsilon}_L} \tag{95}$$

The left-hand side of the above equation expresses the outflux of probability for the configuration $\{\epsilon_1 \cdots \epsilon_i \cdots \epsilon_L\}$, while the right-hand side expresses the influx. Our fundamental goal is to solve Eq. (95).

First, multiply Eq. (95) by ϵ_j and sum over $\{\epsilon\}$. We must separate this into three calculations: (i) that for $1<j<L$, (ii) the boundary term $j=1$, and (iii) the boundary term $j=L$.

Consider case (i): Eq. (95) then gives

$$L\langle \epsilon_i \rangle = (L-3)\langle \epsilon_i \rangle + \langle \bar{\epsilon}_i \rangle + \langle \bar{\epsilon}_i \bar{\epsilon}_{i+1} \rangle + \langle \bar{\epsilon}_i \rangle - \langle \bar{\epsilon}_{i-1} \bar{\epsilon}_i \rangle + \langle \epsilon_i \rangle \ . \tag{96}$$

To simplify this equation, we use two identities

$$\langle \epsilon_i \rangle + \langle \bar{\epsilon}_i \rangle \equiv 1 \tag{97}$$

and

$$\langle \bar{\epsilon}_i \bar{\epsilon}_j \rangle \equiv \langle (1-\epsilon_i)(1-\epsilon_j) \rangle = 1 + \langle \epsilon_i \epsilon_j \rangle - \langle \epsilon_i \rangle - \langle \epsilon_j \rangle \ . \tag{98}$$

Thus Eq. (96) can be written as

$$\langle \epsilon_{i+1} \rangle - 2\langle \epsilon_i \rangle + \langle \epsilon_{i-1} \rangle = \langle \epsilon_i \epsilon_{i-1} \rangle + \langle \epsilon_{i-1} \epsilon_i \rangle \ , \quad i=2, \ldots, L-1 \ . \tag{99}$$

Notice immediately that the left-hand side of Eq. (99) is precisely a discrete diffusion, again exposing the similarity of our process to a fluid situation.

Case (ii) reads

$$L\langle \epsilon_1 \rangle = (L-2)\langle \epsilon_1 \rangle + \langle \bar{\epsilon}_1 \rangle - \langle \bar{\epsilon}_1 \bar{\epsilon}_2 \rangle + \langle \epsilon_1 \rangle \tag{100}$$

which, by using Eqs. (97) and (98), is

$$\langle \epsilon_2 \rangle - \langle \epsilon_1 \rangle = \langle \epsilon_1 \epsilon_2 \rangle \ , \tag{101}$$

a discrete zero derivative boundary condition on the free end of the sandpile.

Finally, case (iii) reads

$$L\langle \epsilon_L \rangle = (L-2)\langle \epsilon_L \rangle + \langle \bar{\epsilon}_L \rangle - \langle \bar{\epsilon}_{L-1} \bar{\epsilon}_L \rangle + \langle \bar{\epsilon}_L \rangle \tag{102}$$

or

$$1 - 3\langle \epsilon_L \rangle + \langle \epsilon_{L-1} \rangle = \langle \epsilon_{L-1} \epsilon_L \rangle \ . \tag{103}$$

Notice that this equation can be derived from Eq. (99) by substituting $i=L$, and using the boundary condition

$$\epsilon_{L+1}=1 \ . \tag{104}$$

Now to obtain the drop number distribution. We have not succeeded in a full solution of Eq. (95), and so here offer a mean-field solution. Proceeding in the spirit of Reynolds, we shall obtain the first term in an infinite hierarchy and force closure in the zero correlation approximation:

$$\langle \epsilon_i \epsilon_j \rangle = \langle \epsilon_i \rangle \langle \epsilon_j \rangle (1-\delta_{ij}) + \langle \epsilon_i \rangle \delta_{ij} \ . \tag{105}$$

For simplicity of notation, define

$$Y_i = \langle \epsilon_i \rangle \ . \tag{106}$$

We then obtain from Eq. (99) in the zero correlation [Eq. (105)] approximation

$$Y_{i+1} + Y_{i-1} = \frac{2Y_i}{1-Y_i} \tag{107}$$

or

$$Y_{i+1} - 2Y_i + Y_{i-1} = \frac{2Y_i^2}{1-Y_i} \ . \tag{108}$$

The form Eq. (108)—a discrete second derivative—bears a diffusionlike resemblance to a fluid system, further satisfying interest in this model. Similarly, applying the zero correlation approximation to Eqs. (101) and (103) leads to

$$Y_L - Y_1 = Y_1 Y_2 \ , \tag{109}$$

$$Y_2 = \frac{Y_1}{1-Y_1} \ , \tag{110}$$

together with the familiar boundary condition

$$Y_{L+1}=1 \ . \tag{111}$$

A closed-form solution to Eq. (108) is unavailable. In fact, Eq. (108) determines an area-preserving map, whose fixed point has a degenerate eigenvector with just one eigenvalue, and requires a special analysis. This is done in Appendix B.

We can, however, by a simple power counting argument, estimate the drop number D behavior. We shall discuss only $D \geq 2$

$$\rho_D = \text{Prob}(D) = k^{-1} \langle \epsilon_{L+1-D} \epsilon_{L+2-D} \rangle \ , \tag{112}$$

where k is a normalization constant (see Appendix B).

Assuming a power-law solution (which we justify in Appendix B), i.e.,

$$Y_i = \frac{a}{i^p} \ , \tag{113}$$

substituting in Eq. (108) gives, for its leading behavior, a value of $p=2$. Thus

$$\rho_D = \frac{\text{const}}{D^4} \ , \tag{114}$$

i.e., a power law with exponent 4. A more detailed derivation is presented in Appendix B, showing that const$=3$ and in particular is explicitly independent of L, and so scale invariant. However, the reader should remember that these equations and results are valid only in the mean-field approximation.

Figures 24 and 25 show results from actual simulations of the LLL model. Notice the successful prediction of a power-law behavior. Least-squares fits to the slope yield -3.31 and -3.59, respectively, as compared to -4 in the mean-field approximation.

Let us formally consider the detailed probability distribution of the configurations themselves. In our mean-field approximation Eq. (105), this is elementary:

$$\pi^{(L)}_{\epsilon_1 \cdots \epsilon_i \cdots \epsilon_L} = \prod_{i=1}^{L} f_i(\epsilon_i) \ , \tag{115}$$

where

$$f_i(\epsilon) = x_i^{\epsilon}(1-x_i)^{1-\epsilon} \tag{116}$$

so that $\langle \epsilon_i \rangle = x_i$. Using Eq. (187) as adequate for the $\langle \epsilon_i \rangle$, we then have

$$\pi^{(L)}_{\epsilon_1 \cdots \epsilon_i \cdots \epsilon_L} \sim \frac{1}{4} \prod_{i=1}^{L} \left[\frac{3}{(L+1-i)(L+5-i)} \right]^{\epsilon_i} . \tag{117}$$

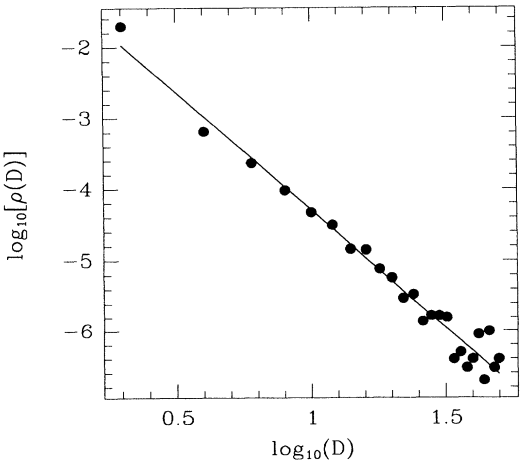

FIG. 24. Results from the LLL model simulations confirming the power-law decay in the probability of drop sizes with increasing size. The power law is less than 4.

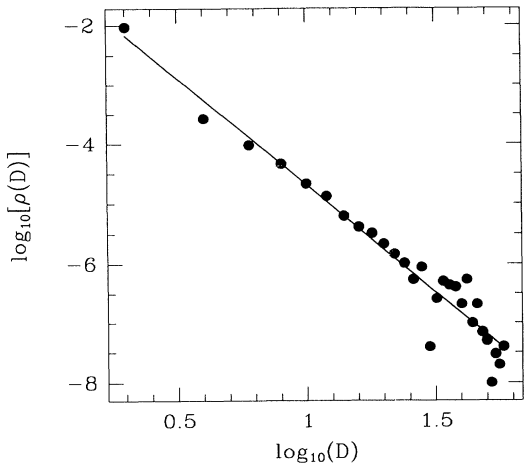

FIG. 25. Results from the LLL model simulations confirming the power-law decay in the probability of drop sizes with increasing size. The power law is less than 4.

Notice that $\pi^{(L)}_{0\cdots 0} \sim \frac{1}{4}$, whereas $\pi^{L}_{1\cdots L} \sim 3^L/(L)^2$, so that different configurations have probabilities more than exponentially different. Next notice that we can write the product form of Eq. (117) in a manner recursively relating $\pi^{(L+1)}$ to π^L:

$$\pi^{(L+1)}_{\epsilon_0 \epsilon_1 \cdots \epsilon_L} \sim \left[\frac{3}{(L+1-i)(L+5-i)} \right]^{\epsilon_0} \pi^{(L)}_{\epsilon_1 \cdots \epsilon_i \cdots \epsilon_L}$$
$$\equiv \sigma_L^{\epsilon_0} \pi^{(L)}_{\epsilon_1 \cdots \epsilon_i \cdots \epsilon_L} \ . \tag{118}$$

By this derivation, we now see that half of all the $\pi^{(L+1)}$ probabilities are just the π^L probabilities, whereas the other half are strongly suppressed by $\sim 1/L^2$. Thus for any large L only a Cantor set survives on which π attains nonvanishing values. Also Eq. (117) informs us that π is log additive:

$$\ln \pi^{(L)} \sim \sum_{i=1}^{L} \epsilon_i \ln \sigma_{L-i} \ , \tag{119}$$

where the multipliers of the ϵ_i are quite variable for large L.

VII. CONCLUSIONS

The local limited model, which at first sight seemed to be rather simple and similar to the exactly solvable Abelian sandpile models, turned out to be exceedingly difficult to solve exactly. The sources of the difficulty were found to be related to the lack of translational invariance and a nontrivial distribution of trapping sites. To better understand the effect of these features we studied two other models each of which had only one of the above two features. The first of which was the PLL model, which has periodic boundary conditions and is translationally invariant. Using this model we were able to develop a scaling theory based on two diverging length scales. The theoretical exponents differed from those computed from simulations by up to 15%. The theory predicts that the LL and PLL models have the same scaling properties in

the thermodynamic limit. The agreement with simulations in the LL model was somewhat better, the maximum error being about 5%. We have not been able to satisfactorily resolve the question as to whether these discrepancies between theory and simulation are due to the presence of exponential corrections and finite-size effects or whether they are due to the presence of additional length scales not taken into account by the theory. We point out that the theory also neglects possible correlations between the spin and trap variables which could be another source of error.

The last model studied was a trapless version of the LL model. This model turns out to have surprisingly rich scaling behavior. While attempting an exact solution of this model we encountered the classic closure problem commonly encountered in fluid mechanics. We believe that this is not a coincidence and that these models dealing with the transport of sand genuinely capture many of the features (and difficulties) of transport problems in fluid mechanics.

The upshot of our calculations are that these models exhibit long-range correlations. However, the probability to see a large excursion from a typical drop number still falls off exponentially, as one might expect from statistical mechanics.

We propose that the origin of the long-range correlations is in the boundary conditions. By maintaining reflecting and absorbing walls at the two ends of the sandpiles one sets up an average flux of particles going from the reflecting to the absorbing ends. A similar setup can be achieved in hydrodynamics by taking a fluid and maintaining it in a box whose two opposite walls have different temperatures. Avoiding convection, one sets up a heat flux going from the hotter to the colder wall. The statistical mechanics of such simple nonequilibrium stationary states exhibit long-range correlations, which disappear altogether if the boundary conditions are relaxed [11,12]. We therefore feel that many of the observed features of self-organization found in these models may be similar to those found in many other systems such as fluids far from equilibrium.

ACKNOWLEDGMENTS

We would like to thank Jean Carlson, Barry Cipra, Jens Eggers, Daniel Fisher, Eric Grannan, Joachim Krug, Sid Nagel, Glen Swindle, Chao Tang, and Reuven Zeitak for useful conversations. This research was supported by the Division of Materials Research of the National Science Foundation, the Israel–U.S. Binational Research Fund, and by the Pew Foundation.

APPENDIX A

Since $H_i \geq i$ for recurrent configurations, it is natural to define

$$X_i \equiv H_i - 1 \tag{A1}$$

so that

$$0 \leq X_i \leq i \tag{A2}$$

for all recurrent states, since $\Delta H \leq 2$ by (A1) is

$$\epsilon_i \equiv X_i - X_{i-1} \leq 1 \ . \tag{A3}$$

A particular configuration is then a sequence $\{X_i\}$, $i=1,\ldots,L$ satisfying (A1)–(A3).

We want to determine N_L, the number of recurrent states for a pile of length L. To do so, it is convenient and informative to partition N_L into $N_{L,K}$ where

$$N_L = \sum_0^L N_{L,K} \tag{A4}$$

with $N_{L,K}$ denoting the configurations for which the last X, $X_L = K$. It now follows from (A3) that

$$N_{L+1,K} = \sum_{M=K-1}^{L} N_{L,M} \ , \tag{A5}$$

where $M > K$ is the contribution from traps at $i = L+1$.

We can now define limited trap depth models as L_r^2, by sharpening (A3) to

$$-r \leq \epsilon_i \leq 1, \quad r=0,1,\ldots \ . \tag{A6}$$

The LLL model corresponds to $r=0$. For those models (A5) becomes

$$N_{L+1,K} = \sum_{k=1}^{k+r} N_{L,M} \ , \tag{A7}$$

where we include values of $M > L$ by modifying $N_{L,K}$ to be

$$N_{L,K} = 0, \quad K<0, \ K>L \ . \tag{A8}$$

We now proceed to sum (A7). First notice that

$$N_{L+1,K} - N_{L+1,K+1} = N_{L,K-1} - N_{L,K+r+1}, \quad K>0 \tag{A9}$$

$$N_{L+1,0} - N_{L+1,1} = -N_{L,r+1} \ . \tag{A10}$$

Let us define some generating functions:

$$\hat{N}_K(Z) = \sum_{L=K}^{\infty} z^L N_{L,K} = z^K + O(z^{k+1}) \ . \tag{A11}$$

Notice by interchanging summations that

$$\hat{N}(z) \equiv \sum_{K=0}^{\infty} \hat{N}_k = \sum_{L=0}^{\infty} z^L N_L \ . \tag{A12}$$

Equations (A9) and (A10) hold only for $L \geq 0$, although both are correct at $L=0$ with the definition

$$N_{0,K} = \delta_{0,K} \ . \tag{A13}$$

Multiplying (A10) by z^{L+1} and summing over $L=0,\ldots,\infty$, paying attention to (A8) and using (A13), produces

$$\hat{N}_0 - \hat{N}_1 = 1 - z\hat{N}_{r+1} \ . \tag{A14}$$

Similarly, for $k>0$, (A9) yields

$$\hat{N}_K - \hat{N}_{K+1} = z(\hat{N}_{K-1} - \hat{N}_{K+r+1}), \quad K>0 \ . \tag{A15}$$

Equation (A15) is linear of order $r+2$ at each fixed value of z, and so its solution is

$$\hat{N}_K=\sum_{i=1}^{r+2} a_i(z)s_i^k(z) \tag{A16}$$

where each s_i satisfies

$$s(1-s)=z(1-s^{r+2}) . \tag{A17}$$

Clearly one root of (A17) is $s(z)\equiv 1$.

As $z\to 0$ there is certainly a root $\hat{s}(z)$ which goes to 0 as z:

$$\lim_{z\to 0}\frac{\hat{s}(z)}{z}=1 . \tag{A18}$$

It is easy to see that this root is unique. Moreover, other than it and $s\equiv 1$, all other roots diverge as $z\to 0$, as the r rth roots of $1/z$. However, $\hat{N}_K$ starts with z^K, and so only $\hat{s}$ can contribute to $\hat{N}_K$ in (A16):

$$\hat{N}_K=\hat{N}_0\hat{s}^K, \quad K\geq 0 . \tag{A19}$$

[$K=0$ has been included, since (A15) at $K=1$ has $\hat{N}_0$, which must enter into the initial values that determine the a_i of (A16).] Substituting (A19) in (A14) yields

$$(1-\hat{s}+z\hat{s}^{r+1})\hat{N}_0=1 ,$$

which by (A17) is

$$\hat{N}_0=\hat{s}/z \tag{A20}$$

and so

$$\hat{N}_K=\frac{1}{z}\hat{s}^{K+1}, \quad K=0,\ldots,\infty , \tag{A21}$$

while by (A13)

$$\hat{N}=\frac{1}{z}\frac{\hat{s}}{1-\hat{s}} . \tag{A22}$$

Equations (A17), (A18), (A21), and (A22) fully determine N_L and $N_{L,K}$ for all r, and it is straightforward to obtain the inverses of these transforms both to yield exact combinatoric formulas for these quantities or, alternatively, their asymptotic forms for $L\to\infty$. To do so, by say (A12),

$$N_L=\frac{1}{2\pi}\oint\frac{dz}{z^{L+1}}\hat{N}(z) \tag{A23}$$

for a sufficiently small contour around $z=0$, since $\hat{N}$ is analytic there. The only impediment is the apparent need to first solve (A17) for $\hat{s}(z)$. This, however, is unnecessary. Since $\hat{s}'(0)=1$ and $\hat{s}$ is analytic at 0, all one needs to do is change variables in (A23) from z to $\hat{s}$, which as an integration variable we will call s. One simply differentiates (A17) and writes by (A17)

$$\frac{1}{z(s)}=\frac{1}{s}\frac{(1-s^{r+2})}{(1-s)}=\frac{(1+s+\cdots+s^{r+1})}{s} . \tag{A24}$$

After integrating by parts, one obtains

$$(L+1)N_L=\frac{1}{2\pi}\oint\frac{ds}{(1-s)^2}\left[\frac{1}{z(s)}\right]^{L+1} , \tag{A25a}$$

and similarly from (A21)

$$\frac{L+1}{K+1}N_{L,K}=\frac{1}{2\pi i}\oint ds\, S^k\left[\frac{1}{Z(s)}\right]^{L+1} , \tag{A25b}$$

where both contours are about $s=0$.

For $r\to\infty$ (the LL model), (A24) simplifies to

$$z(s)=s(1-s) \tag{A26}$$

and all integrations are trivial, producing

$$N_L=C_{L+1}, \quad C_L\equiv\frac{1}{L+1}\binom{2L}{L} \tag{A27}$$

[where $C(L)$ are commonly known as the Catalan numbers] and

$$N_{L,K}=\frac{(K+1)}{(L+1)}\binom{2L-K}{L} , \tag{A28}$$

so that

$$N_{L,0}=N_{L,1}=N_{L-1} . \tag{A29}$$

Rather than obtain further exact formulas for finite r, we obtain asymptotic formulas by steepest descent. In particular $1/z(s)$ has a minimum at s^* satisfying

$$s^{r+2}[1+r(1-r)]=2s-1 \quad (s^* \text{ real}) , \tag{A30}$$

so that as $L\to\infty$, the path $s=s^*+it$ is maximum at s^*. Defining

$$\gamma=1/z(s^*) \tag{A31}$$

and

$$k=\frac{1}{\sqrt{2\pi}}\frac{s^*}{(1-s^*)^2}\left[\frac{1-s^*}{1-r(rs^*-1)}\right]^{1/2} , \tag{A32}$$

we have

$$N_L\sim k\frac{\gamma^{L+1}}{(L+1)^{3/2}}, \quad L\to\infty \tag{A33}$$

with γ increasing from 3 to 4 as r increases above 1 to ∞. Also, by simply comparing (A25) and (A26) we have

$$\frac{N_{L,K}}{N_L}\sim(1-s^*)^2(K+1)s^{*K} \quad L\to\infty, \ K=0,\ldots,\infty \tag{A34}$$

and the terms sum to 1 on K. In particular, all $r>1$ have the property that $N_{L,0}$ is a fixed (large, approaching $\frac{1}{4}$ as $r\to\infty$) fraction of N_L so that all possible configurations are exponentially saturated by those of modest elevations of H_L above its recurrent value of L.

For $r=1$ special care is required since $s^*=1$ in this case (moving towards $\frac{1}{2}$ as r increases), so that (A25) and (A26) require an unintegration by parts and the results are enhanced to

$$N_L\sim\frac{3^{L+1}}{\sqrt{3\pi L}}, \quad \frac{N_{L,0}}{N_L}\sim\frac{3}{2L} . \tag{A35}$$

Notice now that $L\to\infty$, the end of the pile is highly excited in most configurations, so that for kinematic reasons alone, the pile is too "slippery" and cannot sustain the large slopes that the $r>1$ models do.

Finally, $r=0$ is trivial for the enumeration of

configurations. Obviously,

$$N_L = 2^L, \quad N_{L,K} = \left[\frac{L}{K}\right], \tag{A36}$$

so that $N_{L,0}=1$, and most of the pile is at its minimum slope of 1 according to the mean field result, as opposed to $\frac{3}{2}$ of the LL model.

Since (A24) is analytic in r, (A24)–(A26) allow all counting information to be naturally analytically continued in the trap depth limit r. Formulas (A30)–(A34) are correct then for all $r>1$ and $r=1$ is transitional. It is hard to see how the Markov process can fail to reflect this critical transitional behavior of the underlying phase space. It is conceivable that all $r>1$ fall into the same universality class, so that it is especially interesting to solve the $r=1$ model, as well as analytically continuing to the Markov process itself, so that $r=1+\epsilon$ would be available.

APPENDIX B

The mean-field LLL equations are

$$x_{i+1}-2x_i+x_{i-1}=\frac{2x_i^2}{1-x_i}, \quad 1<i<L \tag{B1}$$

$$x_{L+1}=1 , \tag{B2}$$

$$x_2-x_1=x_1x_2 . \tag{B3}$$

Equations (B1) and (B3) determine that x_i monotonically increases with i, and it is easy to verify that $x_1\to 0$ as $L\to\infty$. Thus we can replace (B1) and (B3) by differential versions:

$$\frac{d^2x}{du^2}=\frac{2x^2}{1-x}=2x^2+2x^3+\cdots \tag{B4}$$

and

$$\left.\frac{dx}{du}\right|_1 = x_1^2 . \tag{B5}$$

Equation (B4) has a first integral

$$\left[\frac{dx}{du}\right]^2 - x_1^4 = \tfrac{4}{3}(x^3-x_1^3)+(x^4-x_1^4)+\cdots$$

or

$$\left[\frac{dx}{du}\right]^2 = \tfrac{4}{3}(x^3-x_1^3)+x^4+\cdots . \tag{B6}$$

Define

$$x=x_1\xi . \tag{B7}$$

Then

$$\left[\frac{d\xi}{du}\right]^2 = 4\left[\frac{x_1}{3}\right](\xi^2-1)+x_1^2\xi^4+\cdots . \tag{B8}$$

Calculating to $O(x_1)$ with $\xi \ll 1/x_1$

$$\beta^2 \equiv x_1/3 , \tag{B9}$$

$$\frac{d\xi}{du}\simeq\beta(\xi^3-1)^{1/2} \tag{B10}$$

or

$$\beta(n-1)=\frac{1}{2}\int_1^{\xi_n}\frac{d\zeta}{(\zeta^3-1)^{1/2}}=k-\tfrac{1}{2}\int_{\xi_n}^{\infty}\frac{d\zeta}{(\zeta^3-1)^{1/2}} ,$$

where (B11)

$$k=\tfrac{1}{2}\int_1^{\infty}\frac{d\zeta}{(\zeta^3-1)^{1/2}}$$

$$=\tfrac{1}{6}B(\tfrac{1}{6},\tfrac{1}{2})=\sqrt{\pi}\frac{\Gamma(\frac{3}{4})}{\Gamma(\frac{2}{3})}=1.214\,325\ldots . \tag{B12}$$

For $1\ll\xi_n\ll 1/x_1$ we have

$$\tfrac{1}{2}\int_{\xi}^{\infty}\frac{d\zeta}{(\zeta^3-1)^{1/2}}=\tfrac{1}{2}\int_{\xi}^{\infty}d\xi\,\xi^{-3/2}(1+\tfrac{1}{2}\xi^{-1}\cdots)$$

$$=\frac{1}{\sqrt{\xi}}(1+\tfrac{1}{14}\xi^{-3}\cdots) . \tag{B13}$$

By (B11), since the first integral converges as $\xi\to\infty$ to k, there must be some $n(L)\equiv a$ such that, as $L\to\infty$

$$\beta(a-1)\sim k . \tag{B14}$$

By (B9), since a is known, so is x_1. We shall shortly determine a by asymptotic matching. Substituting (B14) in (B11) and using (B13),

$$\beta(a-n)\sim\frac{1}{\sqrt{\xi_n}}(1+\tfrac{1}{14}\xi_n^{-3}+\cdots) , \tag{B15}$$

$$\xi_n\sim\frac{1}{\beta^2(a-n)^2}[1+\tfrac{1}{7}\beta^6(a-n)^6+\cdots] , \tag{B16}$$

which by (B9) is

$$x_n\sim\frac{3}{(a-n)^2}\left[1+\frac{1}{7}\left[\frac{x_1}{3}\right]^3(a-n)^6+\cdots\right] . \tag{B17}$$

Clearly $a\sim L$ for (B2) to be tenable. It is easy to verify that

$$x_n=\frac{3}{(a-n)^2-1} \tag{B18}$$

is an exact one parameter family of solutions to (B1), which can satisfy (B2) by choosing

$$a=L+3 \tag{B19}$$

and has a leading perturbation behaving as the $(a-n)^6$ form of (B17), although a different sixth-order polynomial which vanishes at $x=L+1$.

For (B18) and (B17) to match, the a of (B19) is that of (B14) and (B17) as well, and so by (B14)

$$x_1\sim\frac{3k^2}{(L+2)^2} \tag{B20}$$

is an asymptotically exact result for (B1)–(B3), while (B8) is asymptotically correct for all large values of x_n.

We will now determine k^{-1}, relating π to p, and so find an asymptotic exact result for Prob$(d=D)$. Since

$$kp=K\pi , \tag{B21}$$

summing over $P_{\epsilon_1\cdots\epsilon_i\cdots\epsilon_L}$,

$$k=\sum_{\{\epsilon\}}\pi_{\epsilon_1\cdots\epsilon_i\cdots\epsilon_L}\langle\epsilon_1\cdots\epsilon_i\cdots\epsilon_L|K|\epsilon_1\cdots\epsilon_i\cdots\epsilon_L\rangle$$
$$=\langle K\rangle_\pi\ . \tag{B22}$$

(From now on all expectation values are with respect to π.) Since

$$K=\sum_1^L(1-Z_iZ_{i+1})\ , \tag{B23}$$

thus

$$\langle K\rangle=\sum_1^L(1-\langle\bar\epsilon_i\bar\epsilon_{i+1}\rangle)\ , \tag{B24}$$

which with $\bar\epsilon_i=1-\epsilon_i$ is

$$\langle K\rangle=\sum_1^L(\langle\epsilon_i\rangle+\langle\epsilon_{i+1}\rangle-\langle\epsilon_i\epsilon_{i+1}\rangle) \tag{B25}$$

or

$$\langle K\rangle=2\sum_1^L\langle\epsilon_i\rangle+1-\langle\epsilon_1\rangle-\sum_1^L\langle\epsilon_i\epsilon_{i+1}\rangle\ . \tag{B26}$$

Equation (B26) can be simplified using the first moment formulas

$$\langle\epsilon_{i+1}\rangle-2\langle\epsilon_i\rangle+\langle\epsilon_{i-1}\rangle=\langle\epsilon_{i-1}\epsilon_i\rangle+\langle\epsilon_i\epsilon_{i+1}\rangle\ , \tag{B27}$$

$$\langle\epsilon_2\rangle-\langle\epsilon_1\rangle=\langle\epsilon_2\epsilon_1\rangle\ , \tag{B28}$$

$$\epsilon_{L+1}=1\ . \tag{B29}$$

Summing (B21) from 2 to L and adding (B28) yields

$$\sum_1^L\langle\epsilon_i\epsilon_{i+1}\rangle=\tfrac{1}{2}\ , \tag{B30}$$

so that

$$k=\langle K\rangle=2\sum_1^L\langle\epsilon_i\rangle+\tfrac{1}{2}-\langle\epsilon_1\rangle\ . \tag{B31}$$

Equation (B31) is exact. [Equations (B27)–(B29) when integrated contain the necessary information needed to establish that $\sum_0^L\text{Prob}(d=D)=1$ and $\langle d\rangle=\frac{1}{2}$, the latter verifying in the p process that the flux of addition equals the flux of drops.] We now employ our mean field result for $\langle\epsilon_i\rangle$,

$$\langle\epsilon_i\rangle\sim\frac{3}{(L+3-i)^2-1}\quad 1\ll i\le L+1 \tag{B32}$$

which suffices to saturate the sum in (B31) as $L\to\infty$,

$$k\sim\tfrac{1}{2}+3\sum_{i=1}^L\frac{2}{(L+3-i)^2-1}$$
$$=\tfrac{1}{2}+3\sum_{i=1}^L\frac{2}{(i+2)^2-1}$$
$$=\tfrac{1}{2}+3\sum_{i=1}^L\left[\frac{1}{i+1}-\frac{1}{i+3}\right] \tag{B33}$$

or

$$k\sim\tfrac{1}{2}+3\left[\tfrac{5}{6}-\sum_{i=L+2}^{L+3}\frac{1}{i}\right]\ , \tag{B34}$$

which implies

$$k\sim 3+O(L^{-1})\ . \tag{B35}$$

Since $k^{-1}=\langle K^{-1}\rangle_p$, the mean transition probability out of the available sites is asymptotically $\frac{1}{3}$, so that in equilibrium relatively few sites are available for addition and the π process relaxes exceedingly slowly. Since

$$\text{Prob}(d=D>1)=k^{-1}\langle\epsilon_{L+1-D}\epsilon_{L+2-D}\rangle_\pi \tag{B36}$$

for small D, in mean field (no correlations) with (B32) and (B35),

$$\text{Prob}(d=D)\sim\frac{3}{[(D+2)^2-1][(D+1)^2-1]}\ . \tag{B37}$$

[1] L. P. Kadanoff, S. R. Nagel, L. Wu, and S. Zhou, Phys. Rev. A **39**, 6524 (1989).
[2] C. H. Liu, H. M. Jaeger, and S. R. Nagel, Phys. Rev. Lett. **62**, 40 (1989).
[3] P. Bak, C. Tang, and K. Wiesenfield, Phys. Rev. Lett. **59**, 381 (1987).
[4] C. Tang and P. Bak, Phys. Rev. Lett. **60**, 2347 (1988).
[5] Deepak Dhar, Phys. Rev. Lett. **64**, 1613 (1990).
[6] Deepak Dhar and S. N. Majumdar, J. Phys. A **23**, 4333 (1990).
[7] J. Carlson, J. Chayes, E. R. Grannan, and G. H. Swindle, Phys. Rev. A **42**, 2467 (1990).
[8] J. Carlson, J. Chayes, E. R. Grannan, and G. H. Swindle, Phys. Rev. Lett. **65**, 2547 (1990).
[9] L. P. Kadanoff, A. B. Chhabra, M. J. Feigenbaum, A. J. Kolan, and I. Procaccia, Phys. Rev. A **45**, 6095 (1992).
[10] J. Krug, J. Stat. Phys. **66**, 1635 (1992).
[11] I. Procaccia, D. Ronis, and I. Oppenheim, Phys. Rev. Lett. **42**, 289 (1979).
[12] D. Ronis, I. Procaccia, and I. Oppenheim, Phys. Rev. A **19**, 1324 (1979).